Journal of Magnetic Resonance 274 (2017) 148–162

Contents lists available at ScienceDirect

Journal of Magnetic Resonance

journal homepage: www.elsevier.com/locate/jmr

Alternating Delays Achieve Polarization Transfer (ADAPT) to heteronuclei in PHIP experiments

Gabriele Stevanato

School of Chemistry, University of Southampton, University Road, Southampton, UK
Institut des Sciences et Ingénierie Chimiques, Ecole Polytechnique Fédérale de Lausanne (EPFL), Lausanne 1015, Switzerland

ARTICLE INFO

Article history:
Received 5 September 2016
Revised 10 October 2016
Accepted 13 October 2016
Available online 25 November 2016

Keywords:
PHIP
Singlet states
Hyperpolarization
Polarization transfer
ADAPT
SLIC
Parahydrogen
Long-lived states

ABSTRACT

A new methodology for producing hyperpolarized ^{13}C nuclei in small organic systems via parahydrogen induced polarization (PHIP) is proposed: ADAPT (Alternating Delays Achieve Polarization Transfer). The theoretical foundation of the process is investigated in some detail and experimental examples demonstrating the viability of the approach are provided as well. The number of adjustable parameters is fewer than most of other conversion schemes. The achieved theoretical heteronuclear polarization is close to unity for any examined magnetic equivalence regime. The duration of the pulse sequence, which was successfully implemented, can be shorter than other established methods reducing possible relaxation losses. The conversion scheme is robust to B_1 inhomogeneities, but more sensitive to off-resonance RF irradiation.

1. Introduction

Hyperpolarization techniques [1–6] are deemed fundamental to overcome the sensitivity limitations of nuclear magnetic resonance (NMR) allowing recording signals enhanced by up to 5 orders of magnitude compared to standard thermal polarization.

One important route is to perform hyperpolarization in aqueous solutions that could be subsequently infused *in vivo* in order to image metabolic reactions [7], as well as the exploitation of the large signal enhancement for an early stage detection or treatment response to therapy in tumors [8,9]. Material and surface characterization could also benefit from enhanced signals [10,11], and in general all scientific strategies using magnetic resonance.

One of the most promising and cost-effective methods is represented by parahydrogen induced polarization (PHIP). In PHIP hydrogen gas enriched in the ^1H para-state, described by an antisymmetric nuclear wave function with respect to the homonuclear spin exchange, reacts with a substrate target system containing a hydrogenable functionality. Upon hydrogenation the proton pair results highly polarized.

However, proton longitudinal relaxation time T_1 in solution is typically in the range of seconds and this sets a major limitation on the available time to use this large polarization [12–14].

An alternative is to transfer singlet parahydrogen spin order to longer lived low gamma nuclei (^{13}C,^{15}N,...) which are then observable for a longer period of time [15]. In general, prolonging the signal lifetime represents a major challenge at the very root of many mainstream research investigations including the area of long-lived spin orders discovered by Levitt [16–23] and also pursued by the groups of Bodenhausen [24,25] and Warren [26,27].

Ways to achieve polarization transfer to slowly decaying nuclei include field cycling transport [28] and methods based on radiofrequency (RF) pulses [15,29–31].

In 1996 Bargon and co-workers adapted the INEPT sequence [32], originally designed to transfer magnetization from ^1H nuclei to a heteronucleus via spin-spin coupling, to create PH-INEPT, PH-INEPT+ and INEPT($+\pi/4$) pulse schemes, which are effective in transferring polarization when the two protons originating from parahydrogenation are in chemically inequivalent positions [33,31].

In 2005 Goldman proposed a novel approach, consisting of strong RF pulses spaced out by carefully chosen intervals [29,30,34], to transfer polarization from parahydrogen to a heteronucleus. In this seminal paper the external magnetic field is assumed low enough to neglect any proton chemical shift difference. Therefore, the three-spin system is of the form AA′X. However, for near equivalent systems, the Goldman scheme is long.

A further generalization has been investigated in 2010 by Kadlecek and co-workers. The theoretical polarization transfer,

E-mail address: Gabriele.Stevanato@soton.ac.uk

http://dx.doi.org/10.1016/j.jmr.2016.10.009
1090-7807/

disregarding the effect of refocussing RF pulses, achieved by the Kadlecek schemes is always close to 100% [35,34].

Ongoing research in our laboratory, recently submitted for publication, has shown that the conversion from para-order to heteronuclear magnetization in a near equivalent system of the form AA′X can be also achieved by means of a SLIC (Spin Lock Induced Crossing) sequence originally designed to access singlet order in pairs of inequivalent homo-nuclei [36].

Here we propose, test and investigate a class of techniques able to achieve heteronuclear polarization transfer faster than the Goldman and Kadlecek methods assuming a pair of chemically equivalent ^{1}H nuclei and a heteronucleus; in the near equivalence limit the theoretical performance is close to 100%, whereas far from magnetic equivalence it is always more than 90% for all the presented cases. The class of pulse sequences is compact and simply consists of a heteronuclear single pulse and a delay repeated m times: $[\alpha_x - \Delta_\alpha]_m$ (see Fig. 2). For near equivalent systems the delay Δ_α is synchronized to the effective precession frequency which depends on the J-coupling network of the system, and the optimal m produces a duration broadly in the range of $1/\Delta J$.

We name this method ADAPT$_\alpha$ (Alternating Delays Achieve Polarization Transfer). It can be used with strong and/or small α RF pulses, when the conversion becomes essentially a DANTE sequence [37,38]. The phase of the strong pulse is assumed to be along x.

In order to endow the reader with a practical recipe, we begin by first describing the examined spin systems, and then the pulse sequence providing an analytical expression for the delay and number of loops to use in the near equivalence regime (for example the system in Fig. 1a).

An experimental validation shows how proton scalar order can be transferred to heteronuclear polarization in thermal fumaric acid and how ADAPT$_\alpha$ has been successfully applied to the polarization transfer to the carbonyl carbon of (unlabelled) dimethyl maleate-d$_6$, obtained by the catalytic reaction of the dimethyl ester of acetylene dicarboxylic acid in acetone-d$_6$ in a PHIP experiment.

A theoretical comparison, via numerical optimization, with other previously proposed methods will show how ADAPT$_\alpha$ typically performs a considerable transfer in a reduced experimental time for molecular systems over a range of diverse magnetic equivalence conditions.

The detailed theoretical analysis, although forming a consistent part of the present investigation, is presented in Appendices A and B for the interested reader.

2. ADAPT parameters under near equivalence regime

2.1. Spin system definition

In order to investigate the polarization transfer via RF irradiation, we model the product molecule by including a pair of chemically equivalent ^{1}H nuclei and a heteronuclear spin. The resulting three-spin system can be classified near magnetic equivalent when the heteronuclear J-coupling imbalance (ΔJ) is smaller than the homonuclear ^{1}H-^{1}H J-coupling, and far from magnetic equivalence in the opposite case. Other nuclear spins in the product molecule, like ^{2}H nuclei (see Fig. 1b), as well as the effect of relaxation processes on the polarization transfer are neglected in a first approximation. The chemical equivalence of proton nuclei is a good approximation for symmetric systems at any magnetic field and it is still acceptable for non-symmetric systems when the external magnetic field is sufficiently low. This convention will be adopted in the analysis below.

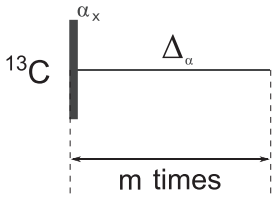

Fig. 2. (a) ADAPT$_\alpha$ (Alternating Delays Achieve Polarization Transfer). The optimal delay and the number of repetitions for near equivalent systems are reported in Table 1.

2.2. Pulse sequence

ADAPT$_\alpha$ pulse sequence is built on a set of three optimal parameters: the flip angle α, the delay Δ_α and the number of loops m. Once the flip angle has been chosen, only two linearly independent parameters are left to be determined: Δ_α and m.

2.3. α, Δ_α and m

We report in Table 1 an analytical expression for the determination of the ADAPT$_\alpha$ parameters in the near equivalence limit.

A general three-step route to determine the right set of parameters, for any magnetic equivalence regime, is provided later in Section Appendix B.5.

We first propose to select the flip angle α. This choice is flexible and depends on the degree of magnetic equivalence of the system under analysis. As a rule of thumb, when $\theta \ll 1$, we suggest the following:

$$\alpha < 180 \quad \text{when} \quad \theta \ll 1: \quad \text{near equivalence} \tag{1}$$

$\alpha = 180$ does not produce any transfer as described in Appendix B.9. In addition, if the system is far from equivalence, large flip angle pulses do not always perform well but the experiment can still be optimized according to the recipe presented below in Section Appendix B.5 using small values of α.

The number of loops m can only be changed in integer steps and a different conversion efficiency may result by adjusting the angle α. Small flip angle pulses also require more repetitions.

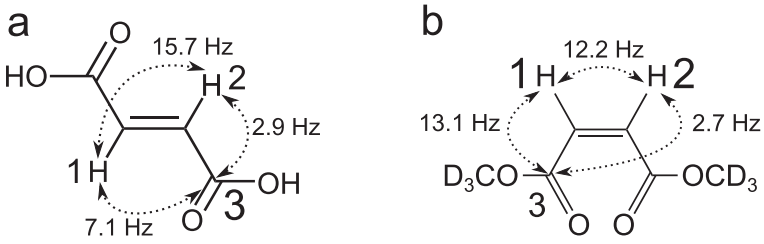

Fig. 1. In panel (a) the molecule of fumaric acid used to validate ADAPT$_\alpha$ via thermal conversion of proton scalar order into ^{13}C transverse magnetization. In (b) the product molecule dimethyl maleate-d$_6$ used in the PHIP experiment to convert para-order into heteronuclear transverse magnetization. The proton nuclei are labelled 1 and 2, whereas 3 indicates the 2% natural abundant ^{13}C nucleus. The assumed J-coupling network is indicated for both systems in Hz.

Table 1
Parameters table for the Δ_α delay and the number of loops for ADAPT$_\alpha$ in the near equivalence limit. $\omega_{eff} = 2\pi\sqrt{J^2 + (\Delta J/2)^2}$ and $\theta = \arctan\left(\frac{\Delta J}{2J}\right)$.

	Parameters for near equivalent systems
Δ_α	$\frac{1}{\omega_{eff}} 2 \arccos\left(\frac{\cos(\alpha/2)\cos(\theta)}{\sqrt{\cos(\alpha/2)^2\cos(\theta)^2+\sin(\alpha/2)^2}}\right)$
m	$\text{Round}\left[\frac{\pi}{2\arccos\left(\frac{1}{2}e^{-i\alpha/2}\left((1+e^{i\alpha})\cos\left(\frac{\Delta\omega_{eff}}{2}\right)+\cos(\theta)(i-i\cos(\alpha)+\sin(\alpha))\sin\left(\frac{\Delta\omega_{eff}}{2}\right)\right)\right)}\right]$

3. Validation

3.1. Thermal experiment

ADAPT$_{90}$ has been applied to transfer polarization from thermal singlet order to the carbonyl carbon on an 8.6 M solution of fumaric acid in DMSO-d$_6$.

Fig. 3a illustrates the heteronuclear conversion result: singlet order, defined as the population imbalance between the singlet and the average triplet proton manifolds, is generated upon application of a SLIC [36] pulse sequence on the proton channel of amplitude $\omega^H_{SLIC} = 2\pi \times 15.7$ rad s^{-1}, and duration $\tau^H_{SLIC} = 335$ ms. The proton and carbon 90 degree pulses are 15.5 μs and 21 μs at 11 W and 9.5 W respectively. A T_{00} filter [39] is subsequently applied to suppress signals not passing through ^{1}H singlet order. Finally, a ^{13}C ADAPT$_{90}$ with $\Delta_{90} = 16.3$ ms and $m = 18$ converts singlet order into heteronuclear magnetization. The ADAPT$_{90}$ parameters have been experimentally optimized to perform optimal transfer. Fig. 3b shows a control experiment as in Fig. 3a, but without the proton SLIC pulse. In Fig. 3c a carbon pulse acquire signal displaying the 1:2:1 triplet structure with a splitting corresponding to the average heteronuclear J-coupling: ~5 Hz.

In the near equivalence regime, the spectrum does not immediately allow to determine the individual heteronuclear J-couplings. The J-coupling imbalance has been coarsely assumed to be $\Delta J = 4.2$ Hz, returning $^2J_{CH} = 2.9$ Hz and $^3J_{CH} = 7.1$ Hz. The number of acquisitions in Fig. 3a and b is 2, in Fig. 3c is 1. Proton singlet order is generated via SLIC in a controlled and reproducible way

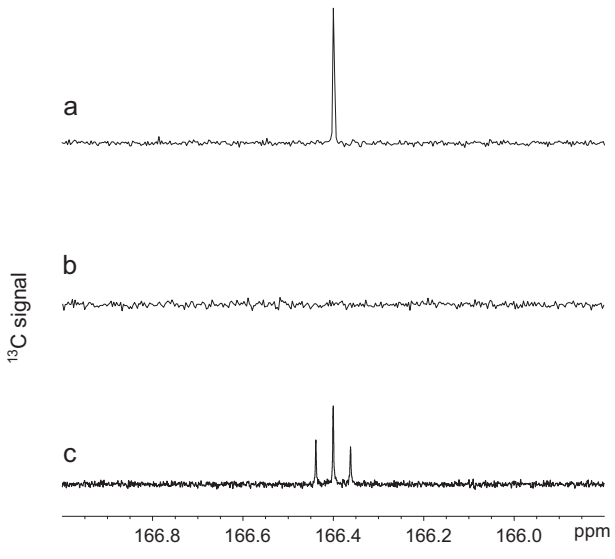

Fig. 3. In panel (a) ^{13}C spectrum of the carbonyl region of fumaric acid upon conversion of ^{1}H singlet order into heteronuclear magnetization. The pulse sequence applied is a 90$_y$-SLIC on the proton channel, followed by a singlet order filter T_{00}, and a ADAPT$_{90}$ on the carbon channel; in panel (b) the same experiment as in (a) but removing the proton SLIC part; in panel (c) 90$_y$ and acquisition on the carbon channel.

in this thermal experiment. In a single-shot PHIP experiment the same control and reproducibility is difficult to achieve.

The theoretical predicted values according to the expression reported in Table 1 for ADAPT$_{90}$ are $\Delta_{90} = 15.9$ ms and $m = 17$. The tiny discrepancy between theoretical and experimental parameters can be attributed to the approximate knowledge of the starting J-coupling network.

Fig. 4 presents a ^{13}C offset dependence investigation of the heteronuclear transfer for fumaric acid. A set of 251 experiments has been performed by varying the ^{13}C offset irradiation in steps of 1 Hz within the range between 20806.87 and 21056.87 Hz in Fig. 4a–c. The interdelay between experiments is 60 s, and the number of acquisitions per point is 2. A SLIC sequence is used to populate proton singlet order as described above. Immediately after T_{00} filtration a conversion scheme is applied to perform heteronuclear transfer. In panel a) ADAPT$_9$ is used with parameters $\Delta_9 = 1.63$ ms and $m = 180$; in panel (b) ADAPT$_{90}$ is used with parameters $\Delta_{90} = 16.3$ ms and $m = 18$; in panel (c) ADAPT$_{162}$ is used with parameters $\Delta_{162} = 28.43$ ms and $m = 12$.

ADAPT$_9$ achieves heteronuclear conversion in the on-resonance region around 20.9 kHz. For ADAPT$_{90}$ other spectral regions with significant hetero-conversion can be identified. The spacing between bands is of the order of $1/\Delta_{90} = 61.3$ Hz. Similarly, the spacing between bands for ADAPT$_{162}$ is about $1/\Delta_{162} = 35.2$ Hz. The analysis of the offset dependence of the heteronuclear conversion is presented in Section Appendix B.11.

3.2. PHIP experiment

ADAPT$_{90}$ and ADAPT$_9$ are applied to achieve heteronuclear polarization transfer in dimethyl maleate-d$_6$. We describe below the experimental preparation method and results. The relevant J-coupling parameters are represented in Fig. 1b.

3.2.1. Preparation

The procedure followed to produce parahydrogen requires room temperature hydrogen gas to flow through a U-shaped metal tube over a charcoal catalyst at 77 K [12,13,5]. At this temperature the hydrogen gas is ~50% enriched in the para-state. Higher para enrichment can be achieved with lower temperatures. For the experiments presented here the hydrogen gas flow was set to 75 mL/min at 77 K. The gas is collected in an aluminium canister and results enriched in the parahydrogen fraction. The hydrogen gas flow was maintained for three hours until the canister pressure reached around 2 bars.

A 5 mM solution of dimethyl acetylene dicarboxylate-d$_6$ and 24 mM of Rh(dppb)(COD) (hydrogenation catalyst, dppb = diphenylphosphinobutane, COD = cyclooctadiene) catalyst, was dissolved in acetone-d$_6$ at room temperature and transferred in two different 5 mm NMR tube subsequently loaded into a 11.75 T NMR magnet. A 1/8″ PFA (perfluoroalkoxy) tubing had been previously inserted into the NMR tube and used to bubble para- H_2 gas from the canister at a rate digitally controlled via a flow meter.

During each polarization transfer experiment parahydrogen was bubbled for 15 s into the NMR sample tube at a flow rate of 25 mL/min. Immediately after bubbling a conversion pulse scheme is applied on the ^{13}C channel on resonance with the ^{13}COO frequency offset. A CW irradiation of 27.7 dB and 1.7 mW, corresponding to a 200 Hz nutation frequency, was applied on the ^{1}H channel while acquiring the ^{13}C signal.

3.2.2. Results

In Fig. 5a is reported the single-transient ^{13}C spectrum of a solution of 5 mM dimethyl ester of acetylene dicarboxylic acid and

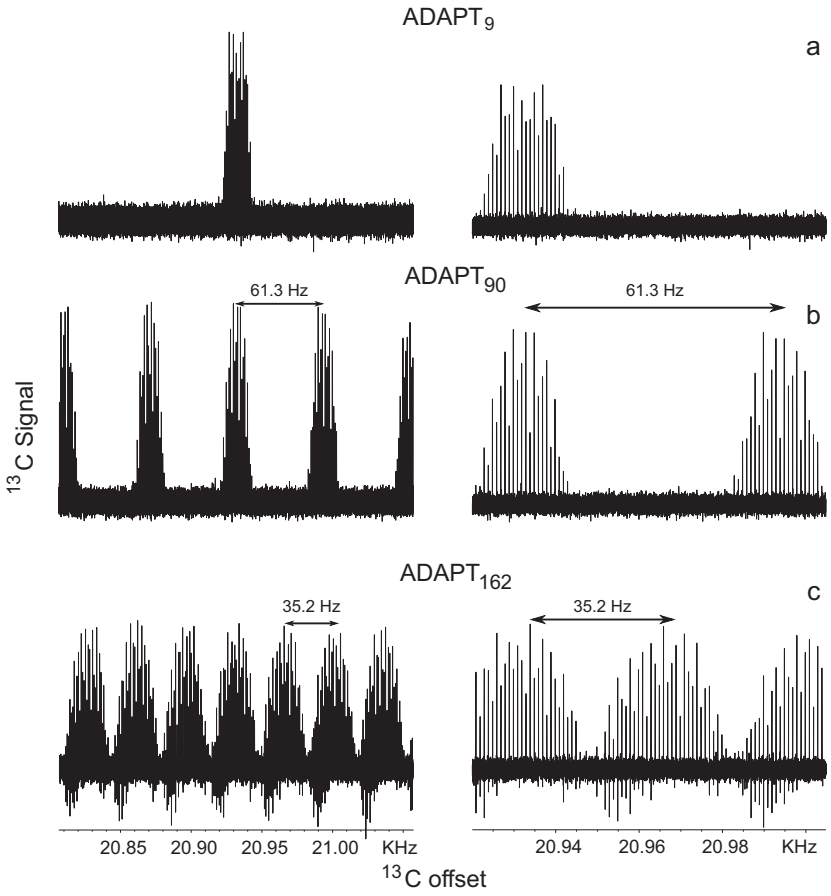

Fig. 4. Offset dependence of the polarization transfer in fumaric acid: panels on the right are just an expansion of the left figures for the region between 20.92 and 21.04 kHz. A set of 251 experiments per panel has been conducted varying the ^{13}C irradiation frequency in step of 1 Hz. The on-resonance frequency is 20931.87 Hz. The conversion schemes used are: in (a) $ADAPT_9$ with $\alpha = 9, \Delta_9 = 1.63$ ms and $m = 180$, in (b) $ADAPT_{90}$ with $\alpha = 90, \Delta_{90} = 16.3$ ms and $m = 18$, and in (c) $ADAPT_{162}$ with $\alpha = 162, \Delta_{162} = 28.43$ ms and $m = 12$. The spectral range investigated is between 20.8 and 21.06 kHz corresponding to ± 1 ppm for ^{13}C at 11.75 T. The theoretical expected polarization transfer is ~83% for $ADAPT_{90}$, ~91% for $ADAPT_{90}$, and ~90% for $ADAPT_{162}$ disregarding relaxation effects. The distance between conversion bands, as predicted in Section Appendix B.11, is indicated for both $ADAPT_{90}$ and $ADAPT_{162}$.

24 mM [Rh(dppb)(COD)]BF4 catalyst in acetone-d_6 before the parahydrogenation reaction. The two peaks at about 29.9 ppm and 206.7 ppm are assigned to the solvent used.

Addition of para enriched hydrogen gas converts the dimethyl ester of acetylene dicarboxylic acid into dimethyl maleate-d_6 which is a symmetric molecule with the two ^1H nuclei sensing the same local magnetic field. Fig. 5b shows the ^{13}C spectrum, after parahydrogenation, averaged over 1024 acquisitions in the ^{13}COO region between 120 and 200 ppm. The inter-delay between consecutive scans was set to 60 s. The multiplet structure at about 133 ppm has been attributed to the catalyst.

The assumed *J*-coupling values for dimethyl maleate-d_6 return the parameters $\theta \simeq 0.4 \simeq 23.08^\circ$ and $\omega_{\text{eff}} \simeq 83.3$ rad s^{-1} as per Eq. (A.8). The parameters $\Delta_{90} = 18.85$ ms and $m = 5$ for the $ADAPT_{90}$ pulse sequence were used. The parameters for $ADAPT_9$ are $\Delta_9 = \Delta_{90}/10$ and $m = 50$.

Fig. 5 in panels (c) and (d) shows the carbonyl region when $ADAPT_{90}$ and $ADAPT_9$ are applied according to the protocol described in Section 3.2.1 immediately after the parahydrogenation reaction respectively. The peak at 165.4 ppm has been assigned to the carbonyl carbon of dimethyl maleate-d_6. The identical duration of $ADAPT_{90}$ and $ADAPT_9$ is 94.25 ms.

The signal enhancement for the ^{13}COO nuclei has been estimated in the range between 665 and 1600 for the investigated conversion schemes.

4. Simulations

4.1. Conversion

Fig. 6a and b shows a numerical simulation of $ADAPT_{90}$, $ADAPT_9$ valid for the system presented in Fig. 1b. The horizontal axis displays the number of loops varied in integer steps, whereas the vertical axis represent the delay used; The delay is indicated as Δ_{90} or Δ_9 for $ADAPT_{90}$ and $ADAPT_9$ in Fig. 2 respectively. The black circle in each panel summarizes the experimental conditions used and described in Fig. 5. An 88% and 92% theoretical efficiency for $ADAPT_{90}$ and $ADAPT_9$ assuming on-resonance irradiation on the ^{13}C spin is predicted.

4.2. Robustness

Simulations in Fig. 6c and d consider the simultaneous incidence of B_1 inhomogeneities and off-resonance RF irradiation for $ADAPT_{90}$, $ADAPT_9$ under the *J*-coupling network presented in Fig. 1b so to address the robustness of the proposed class of methods.

B_1 is varied between $\pm 10\%$ in 1% increments. This means that the flip angle α can vary between 81° and 99° for $ADAPT_{90}$ and 8.1° and 9.9° for $ADAPT_9$. The error on B_1 is also assumed to be systematic, and therefore the angle α does not fluctuate throughout different cycles in $ADAPT_\alpha$.

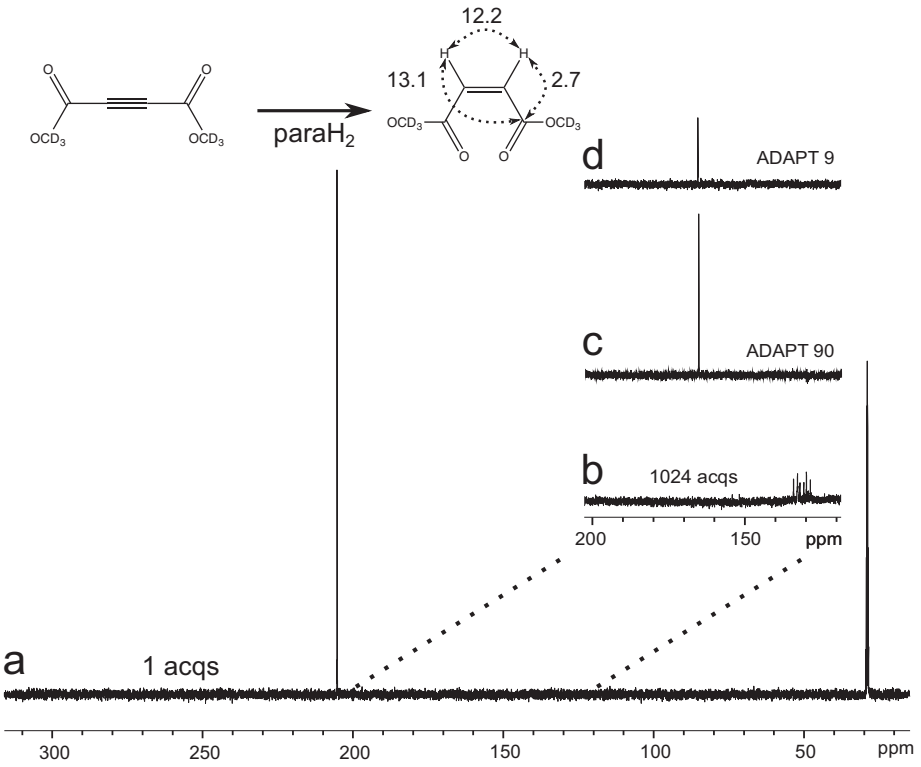

Fig. 5. ^{13}C NMR spectra of the COO site of dimethyl maleate-d_6, obtained by the catalytic reaction of the dimethyl ester of acetylene dicarboxylic acid (at 5 mM concentration) in acetone-d_6 with para-enriched hydrogen, in 11.75 T NMR magnet at 300 K. The assumed *J*-coupling network in Hz is indicated for the product molecule. (a) ^{13}C spectrum with a single-pulse transient in the region 15–325 ppm. Panels (b)–(d) report only the ^{13}C 120–200 ppm spectral region where the COO resonance frequency occurs. In (b) ^{13}C spectrum after 1024 acquisitions. The multiplet structure in the region around 133 ppm is attributed to the [Rh(dppb)(COD)]BF4 catalyst (at 24 mM concentration). Panels (c) and (d) show the ^{13}C spectrum acquired after bubbling the para-enriched hydrogen gas for 15 s and applying in (c) a ^{13}C-ADAPT$_{90}$ with $\Delta_\alpha = 18.85$ ms with 5 repetitions, in (d) a ^{13}C-ADAPT$_9$ with $\Delta_\alpha = 1.885$ ms with 50 repetitions. Every spectrum has a 2 Hz line broadening applied. The NMR signal enhancement factor for the COO resonance peak is ∼665–1600 for ADAPT$_9$ and ADAPT$_{90}$ respectively.

The ^{13}C offset irradiation is varied between ±1 ppm (∼ ±125 Hz at 11.75 T) in steps of 0.01 ppm (∼ ±1.25 Hz). The total number of simulated points per panel is 861. Off-resonance irradiation by ADAPT$_{90}$ in Fig. 6c is characterized by the presence of bands equally spaced out by approximately 0.4 ppm; for ADAPT$_9$ in Fig. 6d the only region representing significant heteronuclear conversion is for on-resonance RF irradiation.

4.3. Numerical simulations of other relevant systems

In order to test the ADAPT$_\alpha$ outside the near equivalence domain, we have numerically simulated some systems reported in Refs. [29,34] and compared the achieved heteronuclear polarization and the conversion time with those performed by Goldman and Kadlecek sequences sketched in Fig. 7.

Table 2 summarizes the results for TMVS (trimethylvinylsilane), TIFBU (trifluoro but-2-enoate), MEPA1/ MEPA2 ([2-(2-Methoxyethoxy) ethyl]ethyl acrylate), SUC (succinic acid), HEP (hydroxyethylpropionate) and BIMAC (2-(2-methoxyethoxy) ethyl acrylate). The *J*-coupling values used in the simulation are reported in Ref. [34] and also presented in Table 2 under the molecule's name. The systems in Table 2 are sorted according to increasing values of θ defined in Eq. (A.8).

For the Goldman sequence in Fig. 7a we used the values reported in Ref. [34] for the timings t_0^G, t_1^G, t_2^G, t_3^G, t_4^G. For Kadlecek2a and Kadlecek2b in Fig. 7b and c the timings t_1^{Ka}, t_2^{Ka}, t_1^{Kb}, t_2^{Kb}, t_3^{Kb}, t_4^{Kb} and number of loops n_3 have been calculated according to equations reported in Ref. [35].

The pulse sequences (a), (b) and (c) in Fig. 7 convert proton singlet population, described by the operator $\frac{1}{8}(\mathbb{1} - 4\mathbf{I_1}\cdot\mathbf{I_2})$, into ^{13}C longitudinal polarization represented by the operator $\frac{I_{3z}}{4}$. The class of ADAPT$_\alpha$ sequences returns directly the transverse ^{13}C polarization $\frac{I_{3x}}{4}$. All numerical calculations were performed by *SpinDynamica*.

5. Discussion

5.1. Parameters determination

A three-step recipe, detailed in Section Appendix B.5, provides the optimal setting to perform a polarization transfer experiment. The strategy used can be applied in any magnetic equivalence regime. Large or small flip angle pulses can be considered. More repetitions are required when using small α excitation pulses.

In the near equivalence limit, when $\theta \ll 1$, the parameters optimization leads to almost 100% heteronuclear conversion, and an analytical expression for the parameters determination has been presented in Table 1. In general, increasing values of θ reduces the possibility of using large flip angle pulses, but a considerable conversion can still be achieved resorting to small α angles (see Table 2). The performance of ADAPT$_\alpha$ worsen in the limit of $\theta \to \pi/2$, and when $\alpha \to \pi$ (see Section Appendix B.9).

5.2. Experimental validation

The thermal experiments presented in Fig. 4 for fumaric acid show the offset dependence of the polarization transfer mecha-

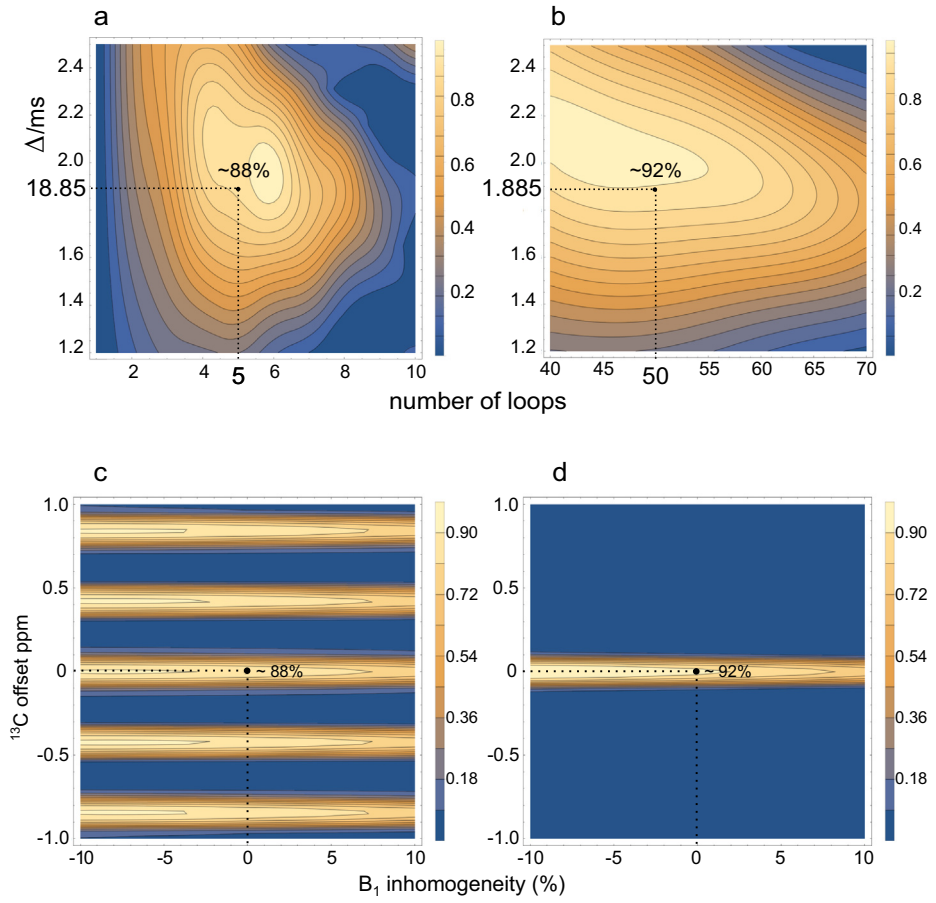

Fig. 6. Polarization transfer countour plots simulating numerically the performance in (a) of ADAPT$_{90}$, and in (b) of ADAPT$_9$ for dimethyl maleate-d$_6$. The coherent evolution Hamiltonian assumes the maleic acid *J*-coupling network indicated in Fig. 1b previously measured. The number of loops is varied in integer steps and no relaxation is included. Heteronuclear conversion efficiency in (c) for ADAPT$_{90}$ and in (d) for ADAPT$_9$ assuming on the horizontal axis a B$_1$ inhomogeneity of ±10%, and an off-resonance ^{13}C irradiation of ±1 ppm on the vertical axis. The black full circle in each panel refers to the experimental condition for experiments in Fig. 5. The number reports the absolute value of the theoretical polarization transferred to ^{13}COO.

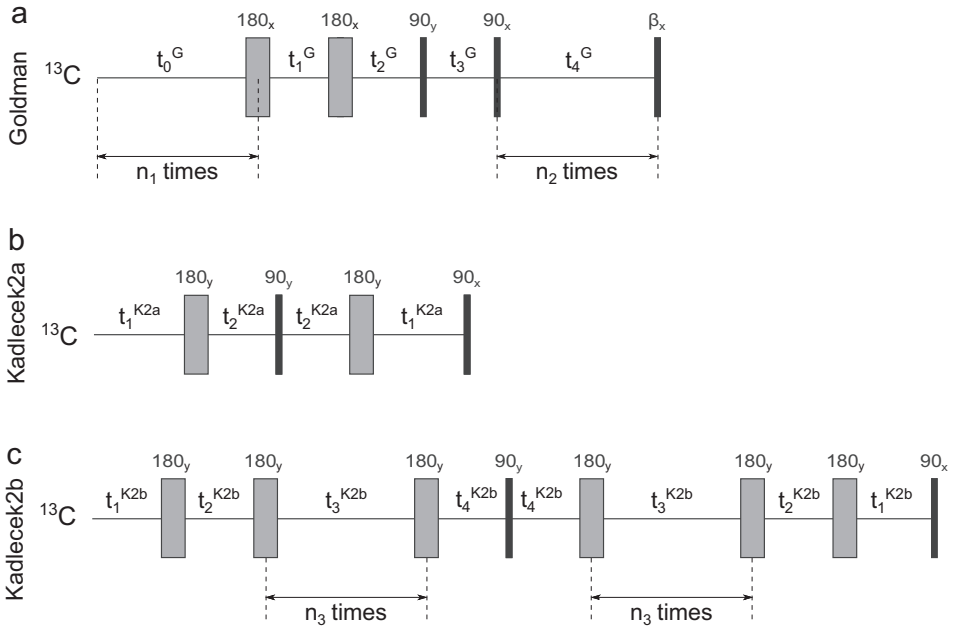

Fig. 7. Pulse sequences to achieve heteronuclear polarization transfer: (a) Goldman, (b) Kadlecek2a, and (c) Kadlecek2b. (a)–(c) are discussed and compared in Ref. [34]. We have not included, unlike in Ref. [34], any refocusing pulse. Sequences (a)–(c) convert singlet population operator into longitudinal ^{13}C polarization $I_{3z}/4$.

Table 2
Numerical simulations comparing ADAPT$_\alpha$ with Goldman and Kadlecek pulse sequences. In particular the delays, number of loops, total duration, and achieved heteronuclear polarization (P) are indicated for TMVS (trimethylvinylsilane), TIFBU (trifluoro but-2-enoate), MEPA1/MEPA2 ([2-(2-Methoxyethoxy) ethyl]ethyl acrylate), SUC (succinic acid), HEP (hydroxyethylpropionate) and BIMAC (2-(2-methoxyethoxy) ethyl acrylate). The J-coupling values in Hz taken from Ref. [34] and the angle θ, defined in Eq. (A.8), are indicated in the first column: the subscripts 1, 2 indicate ^{1}H nuclei and 3 refers to the ^{13}C nucleus.

Molecule θ J (Hz)	Sequence	Timings (ms)	Loops	Duration (ms)	P (%)
TMVS : $\theta = 16.78°$ J_{12}=14.6 J_{13}=15.3 J_{23}=6.5	ADAPT$_{90}$	$\Delta_{90} = 16.84$	m = 8	134.0	99
	Kadlecek2b	$t_1^{Kb} = 22.42$ $t_2^{Kb} = 36.45$ $t_3^{Kb} = 32.79$ $t_4^{Kb} = 8.42$	$n_3 = 1$	200.0	97
	Goldman	$t_0^G = 32.79$ $t_1^G = 18.10$ $t_2^G = 30.76$ $t_3^G = 32.79$ $t_4^G = 32.79$	$n_1 = 2$ $n_2 = 6$	344.0	96
TIFBU : $\theta = 16.90°$ J_{12}=12.5 J_{13}=8.4 J_{23}=0.8	ADAPT$_{90}$	$\Delta_{90} = 19.67$	m = 8	157.4	98
	Kadlecek2b	$t_1^{Kb} = 25.37$ $t_2^{Kb} = 42.79$ $t_3^{Kb} = 38.27$ $t_4^{Kb} = 9.83$	$n_3 = 1$	232.0	97
	Goldman	$t_0^G = 38.27$ $t_1^G = 20.88$ $t_2^G = 36.18$ $t_3^G = 38.27$ $t_4^G = 38.27$	$n_1 = 2$ $n_2 = 6$	401.5	96
MEPA1 : $\theta = 25.09°$ J_{12}=12.6 J_{13}=10.0 J_{23}=−1.8	ADAPT$_{45}$	$\Delta_{45} = 9.81$	m = 8	78.5	98
	Kadlecek2a	$t_1^{Ka} = 29.81$ $t_2^{Ka} = 29.01$		117.6	100
	Goldman	$t_0^G = 29.81$		196.3	96
MEPA2 : $\theta = 35.98°$ J_{12}=12.6 J_{13}=15.8 J_{23}=−2.5	ADAPT$_{90}$	$\Delta_{90} = 17.00$	m = 4	68.0	92
	ADAPT$_{90}$	$\Delta_{90} = 18.20$	m = 10	182.0	100
	Kadlecek2a	$t_1^{Ka} = 12.90$ $t_2^{Ka} = 29.80$		85.5	100
	Goldman	$t_1^G = 20.80$ $t_2^G = 21.71$ $t_3^G = 32.11$		74.6	95
SUC : $\theta = 39.23°$ J_{12}=6.62 J_{13}=4.2 J_{23}=−6.61	ADAPT$_9$	$\Delta_9 = 3.77$	m = 22	83.0	93
	Kadlecek2a	$t_1^{Ka} = 20.10$ $t_2^{Ka} = 54.06$		148.0	100
	Goldman	$t_1^G = 33.96$ $t_2^G = 41.53$ $t_3^G = 58.51$		134.0	98
HEP : $\theta = 40.34°$ J_{12}=7.57 J_{13}=7.24 J_{23}=−5.62	ADAPT$_9$	$\Delta_9 = 3.29$	m = 21	69.0	94
	ADAPT$_{12}$	$\Delta_{12} = 4.75$	m = 15	71.2	95
	Kadlecek2a	$t_1^{Ka} = 16.34$ $t_2^{Ka} = 46.33$		125.0	100
	Goldman	$t_1^G = 28.28$ $t_2^G = 36.20$ $t_3^G = 50.34$		114.8	99
BIMAC : $\theta = 47.83°$ J_{12}=12.00 J_{13}=24.00 J_{23}=−2.5	ADAPT$_9$	$\Delta_9 = 2.1$	m = 18	37.8	100
	Kadlecek2a	$t_1^{Ka} = 5.72$ $t_2^{Ka} = 24.13$		59.7	100
	Goldman	$t_1^G = 13.18$ $t_2^G = 21.38$ $t_3^G = 27.97$		62.5	100

nism via ADAPT$_\alpha$. The ^{13}C offset has been varied in steps of 1 Hz in a spectral region ±1 ppm (∼125.7 Hz) far from the ^{13}C on-resonance condition. The spacing between significant conversion bands depends on the ADAPT$_\alpha$ implemented and is of the order of $1/\Delta_\alpha$ (indicated in Fig. 4 for ADAPT$_{90}$ and ADAPT$_{162}$ and described in Section Appendix B.11).

The spacing between bands can be reduced by setting up an experiment that uses longer delays Δ_α. This can be achieved by implementing in the near equivalence limit an ADAPT$_\alpha$ with large α hard pulses, thus obtaining significant conversion across a large spectral window. ADAPT$_{162}$ in Fig. 4 shows that some significant conversion is achieved across 90% of the region between 20.92 and 21.0 kHz. In the same spectral region ADAPT$_{90}$ and ADAPT$_9$ convert significantly only across 50% and 20% respectively.

This may become important for the class of experiments where a precise offset calibration is difficult. However, whenever the ^{13}C off-resonance offset frequency is $1/(2\Delta_\alpha)$ zero conversion is also expected. As a result, the offset problem is mitigated but not completely eliminated, despite using kHz ^{13}C pulses.

Fig. 5 demonstrates the suitability of ADAPT$_\alpha$ in transferring polarization from parahydrogen to ^{13}COO carbon nuclei in dimethyl maleate-d$_6$ in a PHIP experiment. The signal enhancement in the carbonyl region is 665, 1600 for ADAPT$_9$ and ADAPT$_{90}$ respectively.

Several steps can be optimized to achieve a better polarization transfer, as for example: cooling hydrogen at a lower temperature (a factor of $\sim$3 would be available by enriching the H_2 gas with parahydrogen at 20 K instead of 77 K), using a higher catalyst concentration in the sample preparation, using a higher temperature to foster the catalytic reaction, sustain the proton spin order during para-hydrogenation via decoupling irradiation. In addition, the beginning of the polarization transfer experiment after parahydrogenation was manually triggered. This is surely a source of irreproducibility for an optimal experimental protocol. Once the *J*-coupling network is correctly established for dimethyl maleate-d$_6$, the optimization according to the recipe described in Section Appendix B.5 should lead to improved heteronuclear conversion.

We did not investigate further all of these important practical steps as the primary goal was to demonstrate the polarization transfer possibilities of ADAPT$_\alpha$.

The lower enhancement achieved by ADAPT$_9$ may also suggest an imperfect calibration of the ^{13}C offset as, according to simulations in Fig. 6 and experiments in Fig. 4, this may have a more severe effect when using small flip angle pulses.

All theoretical polarization values reported in the simulation are close or larger than 90%. However, to the best of our knowledge, full conversion has not been achieved experimentally so far. Reported polarization yields range up to a maximum of 50% [30], and for dimethyl maleate-d$_6$, in the present study, the measured polarization is not more than 1%. We assumed for dimethyl maleate-d$_6$ the same *J*-coupling network as for maleic acid. This might be a poor approximation and introduce errors that may crucially affect the transfer.

Moreover, the effect of deuterated parts in the investigated molecular systems is not accounted for in the present model, and no evolution under incoherent effects is analyzed. We did not try to investigate how relaxation impacts the polarization transfer efficiency in this class of experiments.

The distinct advantage of ADAPT$_\alpha$ in the examined cases is to perform more than 90% theoretical polarization transfer faster than other concurrent methodologies; a weakness is the dependence of the transfer on the ^{13}C offset as shown for the thermal conversion of fumaric acid in Fig. 3d.

5.3. Simulations

The simulation in Fig. 6a and b indicate that other values for Δ_{90} and Δ_9 may produce a more favourable theoretical polarization transfer, higher than 88% or 92%. The reason for reporting these values is that the experimental session came first and we were only concerned in showing that a transfer was possible rather than optimizing it. The subsequent theoretical formalization showed that the optimal Δ_{90} differs in general from $\pi/2\omega_{\text{eff}}$, initially guessed.

For example if the $\alpha = \frac{3\pi}{5}$, an ADAPT$_{108}$ with $\Delta_{108} = 23.56$ ms and $m = 5$ is expected to achieve a theoretical conversion of >99%.

In the simulations presented in Fig. 6c and d, if on-resonance irradiation (^{13}C reference offset equal to zero) is considered the theoretical hetero-nuclear polarization transfer ranges between 72% and 90% for a variation of B_1 in the range $\pm$10%.

The presence of significant hetero-nuclear conversion in some well-defined off-resonance regions in the range $\pm$1 ppm for different ADAPT$_\alpha$ schemes is analyzed in Section Appendix B.11.

Essentially a replica of the on-resonance conversion pattern is expected whenever:

$$\omega_{\text{off}}\Delta_\alpha = 2k\pi \quad \text{for} \quad k = 0, \pm 1, \pm 2 \ldots \tag{2}$$

For the PHIP product molecule $\Delta_{90} = 18.85$ ms and the first bands for $k = \pm 1$ are anticipated when:

$$\omega_{\text{off}} = 2\pi\nu_{\text{off}} = \pm 2\pi \frac{10^3}{18.85} = \pm 2\pi \times 53.05 \text{ Hz} \tag{3}$$

$\nu_{\text{off}} = 53.05$ Hz corresponds to about 0.42 ppm in a at 11.75 T magnet as the one used in our experiments and assumed in simulations. On the contrary ADAPT$_9$ in Fig. 6 seems to display heteronuclear conversion only on-resonance.

According to the justification in Section Appendix B.11: $\Delta_9 = 1.885$ ms is ten times smaller than Δ_{90} and the first off-resonance conversion bands are expected, according to Eq. (2), at $\pm$4.2 ppm away from the resonance offset.

Although both ADAPT$_{90}$ and ADAPT$_9$ are predicted to achieve significant heteronuclear polarization transfer, the robustness to offset imperfections is better when using 90° (or larger as can be seen for fumaric acid in Fig. 4) pulses rather than small flip angles.

Simulations seem also to indicate that for ADAPT$_{90}$ using pulse angles about 5% smaller may improve the polarization transfer of few percent for this specific *J*-coupling network.

Overall the correct offset determination is paramount to the success of the polarization transfer: Fig. 6 suggests that an off-resonance irradiation of 0.25 ppm corresponding to about 30 Hz at 11.75 T produces a loss of more than 70% in the polarization transfer irrespective on the B_1 inhomogeneities.

If working on resonance on the ^{13}C channel (or at the centre of the side bands) the loss in polarization transfer for B_1 imperfections is up to a maximum of about 30% for a 10% aberration of the RF pulse.

5.4. ADAPT$_\alpha$ vs Kadlecek and Goldman sequences

Table 2 compares ADAPT$_\alpha$ to Goldman and Kadlecek pulse sequences indicated in Fig. 7 for some molecular ensembles assuming ^{1}H chemical equivalence.

A magnetic inequivalent system is characterized by a large θ value, defined in Eq. (A.8), as for the molecules SUC, BIMAC and HEP. Although for these systems Goldman and Kadlecek schemes achieve the highest polarization transfer, ADAPT$_9$ can theoretically transfer about 93% of polarization in SUC ($\theta = 39.23$) in about 80 ms, i.e. 40–45% faster than Kadlecek2a and Goldman sequences. Similarly, for HEP ($\theta = 40.34$) a conversion of about 95% is achieved for ADAPT$_{12}$ in 71.25 ms compared to 100% of Kadlecek2a in 125 ms and 99% of Goldman in 114.82 ms. In addition, ADAPT$_{90}$ achieves a theoretical 92% of polarization transfer in MEPA2 ($\theta = 35.9$) in 68 ms, whereas Kadlecek2a reaches 100% in 85.5 ms and Goldman completes 95% in 74.62 ms. We also report a 100% of polarization transfer in MEPA2 for ADAPT$_{90}$ in 181.25 ms, i.e. slower than Kadlecek2a and Goldman.

Other simulated systems are less magnetic inequivalent: TMVS ($\theta = 16.78$), TIFBU ($\theta = 16.9$), MEPA1 ($\theta = 25.09$). In particular for TMVS a 98% conversion is achieved by ADAPT$_{90}$ in 134.0 ms versus 97% of Kadlecek2b in 200 ms and 96% of Goldman in 343.97 ms. Therefore, ADAPT$_{90}$ is about 35% and 60% faster than Kadlecek2b and Goldman respectively. Identical figures in terms of polarization and transfer duration are found for TIFBU, which indeed has a very similar θ parameter. Finally, for MEPA1 ($\theta = 25.09$), ADAPT$_{45}$ achieves 98% polarization transfer in 78.5 ms. Kadlecek2a and Goldman achieve 100% and 96% in 117.6 ms and 196.34 ms respectively.

A possible inconvenience of using sequences looped multiple times is that the repetition can obviously only be implemented in integer steps preventing in some cases full theoretical polarization conversion.

The computational effort to optimize ADAPT$_\alpha$ is minimal: a single timing Δ_α, and an integer parameter m. A total of two independent parameters rather than 5 timings, 2 loops and 1 angle in Goldman sequence or 4 timings and 2 integer loops in Kadlecek2b. On the other hand Kadlecek2a requires also to set only two timings.

In summary numerical simulations suggest that an equal or better polarization transfer is achieved by ADAPT$_\alpha$ in nearly magnetic equivalent systems in a shorter time compared to Kadlecek and Goldman schemes. A very good performance of more than 90% polarization conversion is also predicted far from magnetic equivalence in a much reduced experimental time compared to other methods.

6. Conclusion

We have demonstrated the transfer of nuclear spin polarization from parahydrogen to ^{13}COO nuclei in dimethyl maleate-d$_6$ by applying ADAPT$_\alpha$ with $\alpha = 90, 9$. We also have shown that ADAPT$_\alpha$ may be used to convert ^{1}H singlet order into heteronuclear ^{13}C transverse magnetization in fumaric acid. The ADAPT$_\alpha$ is a simple and compact procedure involving loops of α RF pulses and delays. In the limit of a small flip angle α ADAPT$_\alpha$ is a DANTE sequence, but is serviceable to achieve polarization transfer even with strong 90° (or larger) RF pulses. However, the performance decreases when $\alpha \to \pi$. The methodology is based on the optimization of the inter-delay between pulses and the number of loops to perform.

An analytic description of ADAPT$_\alpha$ is presented in the appendix, emphasizing the geometrical character of the spin evolution. In addition, numerical simulations, by comparing ADAPT$_\alpha$ to Goldman and Kadlecek schemes, illustrate the applicability of the method even far from magnetic equivalence. The methodology is generally applicable with a theoretical polarization transfer performance, in all investigated cases, higher than 90%. In particular in the near equivalence limit, for the investigated cases, ADAPT$_\alpha$ achieves the largest polarization transfer in the shortest time.

When ADAPT$_\alpha$ is applied with small flip angles, more repetitions are needed for near equivalent systems. If the number of loops required by ADAPT$_\alpha$ is less than one, the user can try to implement a ADAPT$_{\alpha'}$ with $\alpha' < \alpha$.

An experimental investigation on fumaric acid shows the heteronuclear offset dependence of the proposed method for ADAPT$_9$, ADAPT$_{90}$, ADAPT$_{162}$. The dependence of ADAPT$_{90}$ and ADAPT$_9$ to B$_1$ inhomogeneities and ^{13}C offset imperfections for dimethyl maleate-d$_6$ is also numerically presented. The impact of off-resonance ^{13}C irradiation on the polarization transfer, for near equivalent systems, can be mitigated by resorting to stronger RF pulses.

The simplicity of the ADAPT$_\alpha$ sequence, the small number of parameters to optimize and the applicability in diverse conditions of magnetic equivalence could favour the dissemination of the method. The proposed scheme achieves significant heteronuclear transfer faster than other examined strategies.

ADAPT$_\alpha$ might prove to be important when transferring polarization at longer proton distances where the difference in heteronuclear J-coupling is increasingly small, and at low magnetic fields where the homonuclear difference in chemical shift is minimized even for non symmetric systems.

Acknowledgement

This research was supported by the Engineering and Physical Sciences Research Council (UK), (Grant Nos. EP/M508147/1, EP/N002482/1, EP/L505067/1). I thank Giuseppe Pileio, Salvatore Mamone, Christian Bengs, Stuart Elliott, Karel Kouřil, Benno Meier for useful insights and discussions; James Eills, William Hale, Stefan Glöggler, Javier Alonso-Valdesueiro for experimental help; James Eills, Giuseppe Pileio, Jean-Nicolas Dumez and Malcolm Levitt for reading the manuscript prior to submission. Most of the work in this article employed the *SpinDynamica* code for Mathematica, programmed by Malcolm H. Levitt, with contributions from Jyrki Rantaharju, Andreas Brinkmann, and Soumya Singha Roy, available at www.spindynamica.soton.ac.uk.

Appendix A. Theory

We present a model for understanding and predicting how the high parahydrogen polarization can be efficiently transferred to the ^{13}C nuclei in a three-spin system for observation. The proton nuclei are assumed chemically equivalent.

The theoretical result can be applied to analyse either the experiment regarding the parahydrogenation of dimethyl acetylene dicarboxylate-d$_6$ and Rh(dppb)(COD) presented in Section 3.2 and those concerning other, more general, asymmetric molecular systems when the external static magnetic field B$_0$ is sufficiently low to disregard any chemical shift difference between like nuclei.

We begin by modelling the product molecule in Fig. 1b as a system formed by two ^{1}H and one ^{13}C nuclei prototyping a quantum mechanical nuclear spin ensemble in solution. Other nuclear spins, such as the deuteron nuclei, are neglected.

The labels 1, 2 and 3 in Fig. 1b indicate the two protons and the carbon nuclei respectively. The analysis below includes the following steps: definition of the coherent nuclear spin Hamiltonian and its matrix representation in a convenient symmetrized basis set; identification of the four 2×2 subspaces allowing the complete representation of the J-coupling Hamiltonian $\mathcal{H}_J$ as a direct sum of independent contributions; the geometrical representation of $\mathcal{H}_J$ (see Fig. A.8); the Hamiltonian evolution superoperator under free evolution and in presence of strong idealized pulses; the geometrical representation of ADAPT$_\alpha$ as trajectory in orthogonal subspaces (see Fig. B.9).

A.1. The coherent Hamiltonian and the symmetrized basis set

Assuming the proton nuclei chemically equivalent, and on-resonance ^{13}C RF irradiation, we write the coherent Hamiltonian in the rotating frame as follows:

$$\mathcal{H}_{\text{coh}} = \mathcal{H}_J$$
$$\mathcal{H}_J = \omega_J \mathbf{I_1} \cdot \mathbf{I_2} + \frac{\omega_\Sigma + \omega_\Delta}{2} I_{1z} I_{3z} + \frac{\omega_\Sigma - \omega_\Delta}{2} I_{2z} I_{3z} \tag{A.1}$$

where $\omega_J = 2\pi J_{12}, \omega_\Sigma = 2\pi(J_{13} + J_{23})$ and $\omega_\Delta = 2\pi(J_{13} - J_{23})$. A convenient *symmetrized* basis set $\mathbb{STX}$ to represent Eq. (A.1) is formed by the direct product of the singlet-triplet basis for ^{1}H spins 1 and 2, and the eigenbasis for the I_{3x} operator of ^{13}C spin 3:

$$\mathbb{STX} = ST_{\{1,2\}} \otimes X_3 \tag{A.2}$$

A member of $\mathbb{STX}$ is for example $-(|\, S^0_{1,2}\rangle\otimes|\, \alpha_3\rangle - |\, S^0_{1,2}\rangle\otimes|\, \beta_3\rangle)$.

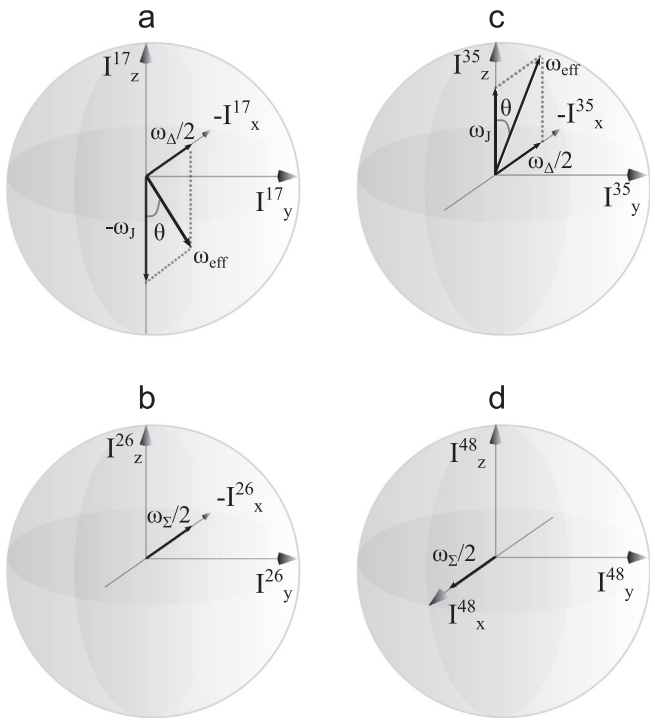

Fig. A.8. Geometric representation of $H^{17}, H^{26}, H^{35}, H^{48}$ in panels (a)–(d) respectively. The evolution in the subspaces 17 and 35 is an effective rotation with angular velocity ω_{eff} about an axis tilted by an angle θ from the relative z direction.

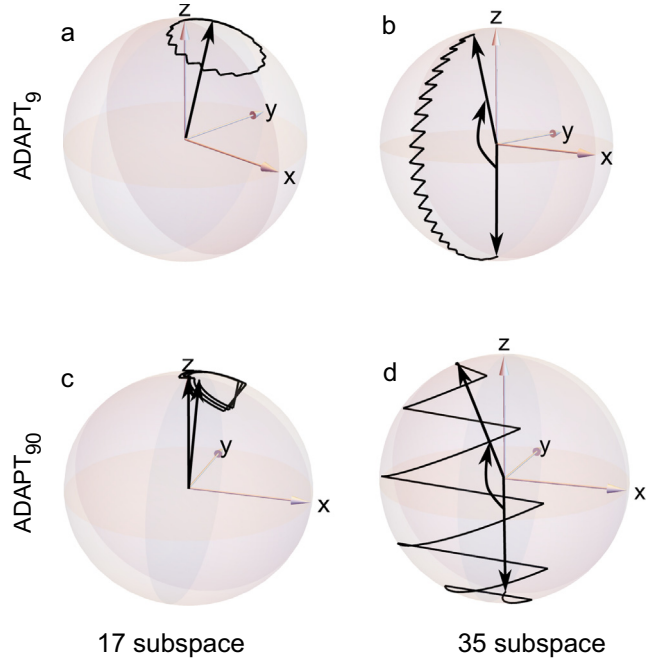

Fig. B.9. Evolution in (a) of the vector I_z^{17}, and in (b) of the vector $-I_z^{35}$ for an on-resonance ADAPT$_9$ sequence for the far from equivalence system of succinic acid. The SUC J-coupling are listed in Table 2. Parameters used in simulation are $\alpha = \pi/20, \Delta_9 = 3.77$ ms and $m = 22$. The projection $|I_z^{17} + I_z^{35}|$ determines a 93% conversion. Evolution in (c) of the vector I_z^{17}, and in (d) of the vector $-I_z^{35}$ for an on-resonance ADAPT$_{90}$ sequence for the near equivalence system of maleic acid. The J-coupling network is sketched in Fig. 1. The ADAPT$_{90}$ parameters considered are $\alpha = \pi/2$, $\Delta_{90} = 18.85$ ms and $m = 5$. The projection $|I_z^{17} + I_z^{35}|$ amounts to a 88% conversion (see also Fig. 6). Simulation performed with SpinDynamica package.

From now onward, in order to keep the notation lighter, we will drop the subscript labels. $\mathbb{STX}$ is formed by the following 8 ($= 2^3$) elements:

$$
\begin{aligned}
|\,1\rangle &= -(|\,S^0,\alpha\rangle - |\,S^0,\beta\rangle)\\
|\,2\rangle &= -(|\,T^1,\alpha\rangle - |\,T^1,\beta\rangle)\\
|\,3\rangle &= -(|\,T^0,\alpha\rangle - |\,T^0,\beta\rangle)\\
|\,4\rangle &= -(|\,T^{-1},\alpha\rangle - |\,T^{-1},\beta\rangle)\\
|\,5\rangle &= (|\,S^0,\alpha\rangle + |\,S^0,\beta\rangle)\\
|\,6\rangle &= (|\,T^1,\alpha\rangle + |\,T^1,\beta\rangle)\\
|\,7\rangle &= (|\,T^0,\alpha\rangle + |\,T^0,\beta\rangle)\\
|\,8\rangle &= (|\,T^{-1},\alpha\rangle + |\,T^{-1},\beta\rangle)
\end{aligned}
\tag{A.3}
$$

Any operator proportional to I_{3x} will have a diagonal representation in $\mathbb{STX}$: this property is convenient when analyzing the rotation induced on spin coordinates by pulse events as α_x acting on ^{13}C nuclei. The matrix representation of $\mathcal{H}_J$ is not block diagonal, but a visual inspection of Eq. (A.4) reveals that it is the direct sum of 4 orthogonal 2×2 subspaces:

$$
\mathcal{H}_J = \begin{array}{c} \\ \langle 1| \\ \langle 2| \\ \langle 3| \\ \langle 4| \\ \langle 5| \\ \langle 6| \\ \langle 7| \\ \langle 8| \end{array}
\begin{array}{c}
\begin{array}{cccccccc} |1\rangle & |2\rangle & |3\rangle & |4\rangle & |5\rangle & |6\rangle & |7\rangle & |8\rangle \end{array} \\
\begin{pmatrix}
-\frac{3\omega_J}{4} & 0 & 0 & 0 & 0 & 0 & -\frac{\omega_\Delta}{4} & 0 \\
0 & \frac{\omega_J}{4} & 0 & 0 & 0 & \frac{-\omega_\Sigma}{4} & 0 & 0 \\
0 & 0 & \frac{\omega_J}{4} & 0 & -\frac{\omega_\Delta}{4} & 0 & 0 & 0 \\
0 & 0 & 0 & \frac{\omega_J}{4} & 0 & 0 & 0 & \frac{\omega_\Sigma}{4} \\
0 & 0 & -\frac{\omega_\Delta}{4} & 0 & -\frac{3\omega_J}{4} & 0 & 0 & 0 \\
0 & -\frac{\omega_\Sigma}{4} & 0 & 0 & 0 & \frac{\omega_J}{4} & 0 & 0 \\
-\frac{\omega_\Delta}{4} & 0 & 0 & 0 & 0 & 0 & \frac{\omega_J}{4} & 0 \\
0 & 0 & 0 & \frac{\omega_\Sigma}{4} & 0 & 0 & 0 & \frac{\omega_J}{4}
\end{pmatrix}
\end{array}
\tag{A.4}
$$

$$
\mathcal{H}_J = H^{17} \oplus H^{26} \oplus H^{35} \oplus H^{48}, \tag{A.5}
$$

where the superscripts r, s in H^{rs} refer to the pair of eigenkets $|\,r\rangle$ and $|\,s\rangle$, reported in Eq. (A.3). For every subspace a set of *single transition operators*, with cyclic commutation relationships $[I_x^{rs}, I_y^{rs}] = iI_z^{rs}$, can be defined:

$$
I_x^{rs} = \begin{array}{c} \\ \langle r| \\ \langle s| \end{array}
\begin{array}{c}
\begin{array}{cc} |r\rangle & |s\rangle \end{array} \\
\begin{pmatrix} 0 & 1/2 \\ 1/2 & 0 \end{pmatrix}
\end{array}
\qquad
I_y^{rs} = \begin{array}{c} \\ \langle r| \\ \langle s| \end{array}
\begin{array}{c}
\begin{array}{cc} |r\rangle & |s\rangle \end{array} \\
\begin{pmatrix} 0 & -i/2 \\ i/2 & 0 \end{pmatrix}
\end{array}
\tag{A.6}
$$

$$
I_z^{rs} = \begin{array}{c} \\ \langle r| \\ \langle s| \end{array}
\begin{array}{c}
\begin{array}{cc} |r\rangle & |s\rangle \end{array} \\
\begin{pmatrix} 1/2 & 0 \\ 0 & -1/2 \end{pmatrix}
\end{array}
\qquad
E^{rs} = \begin{array}{c} \\ \langle r| \\ \langle s| \end{array}
\begin{array}{c}
\begin{array}{cc} |r\rangle & |s\rangle \end{array} \\
\begin{pmatrix} 1 & 0 \\ 0 & 1 \end{pmatrix}
\end{array}
$$

In the notation I_j^{rs}, rs is always one of the pairs in the set $S = \{17, 26, 35, 48\}$ for all j in the set $\{x, y, z\}$. E^{rs} is the identity operator in the rs subspace for $rs \in S$.

It is of practical importance to note that a fictitious spin-1/2 for each individual subspace mimics the trajectory of the system, and that each individual subspace can be monitored independently.

The Hamiltonian operators H^{rs} (with $rs \in S$) in Eq. (A.5) can be equivalently expressed using the single transition operators of Eq. (A.6) as:

$$H^{17} = -\omega_J I_z^{17} - \frac{\omega_\Delta}{2} I_x^{17} - \frac{\omega_J}{4} E^{17}$$
$$H^{26} = -\frac{\omega_\Sigma}{2} I_x^{26} + \frac{\omega_J}{4} E^{26}$$
$$H^{35} = \omega_J I_z^{35} - \frac{\omega_\Delta}{2} I_x^{35} - \frac{\omega_J}{4} E^{35}$$
$$H^{48} = \frac{\omega_\Sigma}{2} I_x^{48} + \frac{\omega_J}{4} E^{48} \tag{A.7}$$

The geometrical representation in Fig. A.8, shows how the evolution in the subspaces 17 and 35 is an effective rotation with angular frequency ω_{eff} about an axis tilted by θ from the vertical direction. As a result H^{17} and H^{35} in Eq. (A.7) can be reformulated in the following way:

$$H^{17} = -\omega_{\text{eff}} \widehat{R}_y^{17}(\theta) I_z^{17} - \frac{\omega_J}{4} E^{17}$$
$$H^{35} = \omega_{\text{eff}} \widehat{R}_y^{35}(\theta) I_z^{35} - \frac{\omega_J}{4} E^{35} \qquad \text{with,}$$
$$\theta = \arctan\left(\frac{\omega_\Delta}{2\omega_J}\right)$$
$$\omega_{\text{eff}} = \sqrt{\omega_J^2 + \left(\frac{\omega_\Delta}{2}\right)^2} \tag{A.8}$$

where $\widehat{R}_y^{rs}(\theta)$ is the rotation superoperator acting on the operator I_z^{rs} and performing a θ rotation about the y axis of the rs subspace for $rs \in \{17, 35\}$.

A.2. Temporal evolution

The temporal free evolution of the spin system can be determined, according to the Liouville Von-Neumann equation, by direct exponentiation of the terms in Eq. (A.7):

$$\widehat{U}(\Delta_\alpha) = \widehat{U}^{17}(\Delta_\alpha)\widehat{U}^{26}(\Delta_\alpha)\widehat{U}^{35}(\Delta_\alpha)\widehat{U}^{48}(\Delta_\alpha)$$
$$\widehat{U}^{rs}(\Delta_\alpha) = e^{-iH^{rs}\Delta_\alpha} \qquad \text{with } rs \in S \tag{A.9}$$

By taking advantage of the following identity:

$$e^{-i\omega_{\text{eff}}\Delta_\alpha \widehat{R_y^{rs}(\theta)} I_z^{rs}} \equiv \widehat{R}_y^{rs}(\theta)\widehat{R}_z^{rs}(\omega_{\text{eff}}\Delta_\alpha)\widehat{R}_y^{rs}(-\theta) \tag{A.10}$$

the propagator for the individual subspaces is:

$$\widehat{U}^{17}(\Delta_\alpha) = e^{i\frac{\omega_J}{4}\Delta_\alpha E^{17}} \widehat{R}_y^{17}(\theta)\widehat{R}_z^{17}(-\omega_{\text{eff}}\Delta_\alpha)\widehat{R}_y^{17}(-\theta)$$
$$\widehat{U}^{26}(\Delta_\alpha) = e^{-i\frac{\omega_J}{4}\Delta_\alpha E^{26}} \widehat{R}_x^{26}\left(-\frac{\omega_\Sigma}{2}\Delta_\alpha\right)$$
$$\widehat{U}^{35}(\Delta_\alpha) = e^{i\frac{\omega_J}{4}\Delta_\alpha E^{35}} \widehat{R}_y^{35}(-\theta)\widehat{R}_z^{35}(\omega_{\text{eff}}\Delta_\alpha)\widehat{R}_y^{35}(\theta)$$
$$\widehat{U}^{48}(\Delta_\alpha) = e^{-i\frac{\omega_J}{4}\Delta_\alpha E^{48}} \widehat{R}_x^{48}\left(\frac{\omega_\Sigma}{2}\Delta_\alpha\right) \tag{A.11}$$

The propagators in Eqs. (A.11) and (A.12) avail us a detailed description of the ADAPT$_\alpha$ pulse sequence.

Appendix B. ADAPT analysis

B.1. Operators

For the investigated dimethyl maleate-d_6, in a first approximation, the state produced upon hydrogenation is the population of the singlet state. This initial state and the observable I_{3x} ^{13}C transverse magnetization are related to the following single transitions operators:

$$|S_0\rangle\langle S_0| = \frac{1}{8}(\mathbb{1} - 4\mathbf{I_1}\cdot\mathbf{I_2}) = \frac{1}{4}(E^{17} - E^{35}) + \frac{1}{2}(I_z^{17} - I_z^{35})$$
$$2(I_{1z}\cdot I_{2z}\cdot I_{3z}) - \frac{I_{3x}}{2} = \frac{1}{2}\left(I_z^{17} + I_z^{35}\right) \tag{B.1}$$

The cartesian representation of I_z^{26} and I_z^{48} contains elements proportional to I_{3x} as well, however the evolution of interest for these subspaces can be neglected as the initial singlet population state, according to Eq. (B.1), has non-zero components only onto the subspaces 17 and 35. Therefore the presented formalization of the pulse sequences is restricted to the subspaces 17 and 35, and we will focus on the evolution of the vectors I_z^{17} and $-I_z^{35}$. We also always assume idealized, instantaneous strong pulses.

By inspecting Eq. (B.1) it is apparent that starting from an initial order proportional to $I_z^{17} - I_z^{35}$ any effective conversion scheme should maximize an operator proportional to $|I_z^{17} + I_z^{35}|$, thus performing a selective inversion in one of the subspaces.

B.2. Coherent evolution

Using Eqs. (A.11) and (A.12), the evolution under a single cycle amounts to the following rotations in subspaces 17 and 35 respectively:

$$\widehat{U}^{17}(\Delta_\alpha)\widehat{U}_\alpha = e^{i\frac{\omega_J}{4}\Delta_\alpha E^{17}} \widehat{R}_y^{17}(\theta)\cdot\widehat{R}_z^{17}(-\omega_{\text{eff}}\Delta_\alpha)\cdot\widehat{R}_y^{17}(-\theta)\cdot\widehat{R}_z^{17}(-\alpha) \tag{B.2}$$
$$\widehat{U}^{35}(\Delta_\alpha)\widehat{U}_\alpha = e^{i\frac{\omega_J}{4}\Delta_\alpha E^{35}} \widehat{R}_y^{35}(-\theta)\cdot\widehat{R}_z^{35}(\omega_{\text{eff}}\Delta_\alpha)\cdot\widehat{R}_y^{35}(\theta)\cdot\widehat{R}_z^{35}(-\alpha) \tag{B.3}$$

The matrix representations of Eqs. (B.2) and (B.3), as a general function of the parameters $\alpha, \Delta_\alpha, \theta, \omega_{\text{eff}}$, in their relative 2×2, 17 and 35 subspaces (disregarding the phase factors) is:

$$\widehat{U}^{17}(\Delta_\alpha)\widehat{U}_\alpha = \begin{pmatrix} e^{\frac{i\alpha}{2}}\left(\cos\left(\frac{\omega_{\text{eff}}\Delta_\alpha}{2}\right) + i\cos(\theta)\sin\left(\frac{\omega_{\text{eff}}\Delta_\alpha}{2}\right)\right) & ie^{\frac{-i\alpha}{2}}\sin(\theta)\sin\left(\frac{\omega_{\text{eff}}\Delta_\alpha}{2}\right) \\ ie^{\frac{i\alpha}{2}}\sin(\theta)\sin\left(\frac{\omega_{\text{eff}}\Delta_\alpha}{2}\right) & e^{\frac{-i\alpha}{2}}\left(\cos\left(\frac{\omega_{\text{eff}}\Delta_\alpha}{2}\right) - i\cos(\theta)\sin\left(\frac{\omega_{\text{eff}}\Delta_\alpha}{2}\right)\right) \end{pmatrix}$$

$$\widehat{U}^{35}(\Delta_\alpha)\widehat{U}_\alpha = \begin{pmatrix} e^{\frac{i\alpha}{2}}\left(\cos\left(\frac{\omega_{\text{eff}}\Delta_\alpha}{2}\right) - i\cos(\theta)\sin\left(\frac{\omega_{\text{eff}}\Delta_\alpha}{2}\right)\right) & ie^{\frac{-i\alpha}{2}}\sin(\theta)\sin\left(\frac{\omega_{\text{eff}}\Delta_\alpha}{2}\right) \\ ie^{\frac{i\alpha}{2}}\sin(\theta)\sin\left(\frac{\omega_{\text{eff}}\Delta_\alpha}{2}\right) & e^{\frac{-i\alpha}{2}}\left(\cos\left(\frac{\omega_{\text{eff}}\Delta_\alpha}{2}\right) + i\cos(\theta)\sin\left(\frac{\omega_{\text{eff}}\Delta_\alpha}{2}\right)\right) \end{pmatrix}$$

It can be verified that the $\mathbb{STX}$ matrix representations of a α pulse with phase x on the ^{13}C channel corresponds to clockwise rotations of α about the z axis of each individual subspace respectively:

$$\widehat{U}_\alpha = e^{-i\alpha\widehat{I_{3x}}} = \widehat{R}_z^{17}(-\alpha)\widehat{R}_z^{26}(-\alpha)\widehat{R}_z^{35}(-\alpha)\widehat{R}_z^{48}(-\alpha) \tag{A.12}$$

B.3. Effective rotation angles

We now use the fact that a positive arbitrary rotation by an angle δ about a direction specified by a unitary vector $\mathbf{n} = \{n_x, n_y, n_z\}$ can always be represented by [40,41]:

$$R_{\mathbf{n}}(\delta) = \cos(\delta/2)E - i\sin(\delta/2)\sigma_{\mathbf{n}} \quad \text{with,}$$
$$\sigma_{\mathbf{n}} = n_x\sigma_x + n_y\sigma_y + n_z\sigma_z$$
$$\sigma_i \cdot \sigma_i = 1 \quad \forall i \in \{x,y,z\}$$
$$[\sigma_x, \sigma_y] = i\sigma_z\circlearrowleft \tag{B.4}$$

where $\sigma_i \forall i \in \{x,y,z\}$ are the Pauli matrices, E is the identity matrix and the symbol $\circlearrowleft$ indicates cyclic commutation relationship. The products in Eqs. (B.2) and (B.3) can then be expressed as a single rotation by an angle δ_{eff}^{17} and δ_{eff}^{35} about an axis specified by $\mathbf{n}^{17} = \{n_x^{17}, n_y^{17}, n_z^{17}\}$ and $\mathbf{n}^{35} = \{n_x^{35}, n_y^{35}, n_z^{35}\}$ respectively:

$$\widehat{U}^{17}(\Delta_\alpha)\widehat{U}_\alpha = \widehat{R}_{\mathbf{n}}^{17}(\delta_{\text{eff}}^{17}) \quad \text{and} \quad \widehat{U}^{35}(\Delta_\alpha)\widehat{U}_\alpha = \widehat{R}_{\mathbf{n}}^{35}(\delta_{\text{eff}}^{35}) \tag{B.5}$$

The effective angles δ_{eff}^{17} and δ_{eff}^{35} are:

$$\delta_{\text{eff}}^{17} = 2\arccos\left(\cos\left(\frac{\alpha}{2}\right)\cos\left(\frac{\omega_{\text{eff}}\Delta_\alpha}{2}\right) - \cos(\theta)\sin\left(\frac{\alpha}{2}\right)\sin\left(\frac{\omega_{\text{eff}}\Delta_\alpha}{2}\right)\right) \tag{B.6}$$

$$\delta_{\text{eff}}^{35} = 2\arccos\left(\frac{1}{2}e^{-i\frac{\alpha}{2}}\left((1+e^{i\alpha})\cos\left(\frac{\omega_{\text{eff}}\Delta_\alpha}{2}\right) + \cos(\theta)(i - i\cos(\alpha) + \sin(\alpha))\sin\left(\frac{\omega_{\text{eff}}\Delta_\alpha}{2}\right)\right)\right) \tag{B.7}$$

When ADAPT$_\alpha$ includes m loops, the effective rotation spans an angle $m\delta_{\text{eff}}^{17}$, and $m\delta_{\text{eff}}^{35}$ about the axes $\mathbf{n}^{17}$ and $\mathbf{n}^{35}$ respectively.

B.4. Effective rotation axes

The rotation axes related to δ_{eff}^{17} and δ_{eff}^{35} are also non-trivial functions of $\alpha, \Delta_\alpha, \theta, \omega_{\text{eff}}$ that we report for completeness. The components along x,y,z of $\mathbf{n}^{17}$ are:

$$n_x^{17} = -\frac{\cos\left(\frac{\alpha}{2}\right)\sin(\theta)\sin\left(\frac{\omega_{\text{eff}}\Delta_\alpha}{2}\right)}{\sqrt{1-\left(\cos\left(\frac{\alpha}{2}\right)\cos\left(\frac{\omega_{\text{eff}}\Delta_\alpha}{2}\right) - \cos(\theta)\sin\left(\frac{\alpha}{2}\right)\sin\left(\frac{\omega_{\text{eff}}\Delta_\alpha}{2}\right)\right)^2}}$$

$$n_y^{17} = -\frac{\sin\left(\frac{\alpha}{2}\right)\sin(\theta)\sin\left(\frac{\omega_{\text{eff}}\Delta_\alpha}{2}\right)}{\sqrt{1-\left(\cos\left(\frac{\alpha}{2}\right)\cos\left(\frac{\omega_{\text{eff}}\Delta_\alpha}{2}\right) - \cos(\theta)\sin\left(\frac{\alpha}{2}\right)\sin\left(\frac{\omega_{\text{eff}}\Delta_\alpha}{2}\right)\right)^2}}$$

$$n_z^{17} = \frac{e^{-i\frac{\alpha}{2}}\left(i(-1+e^{i\alpha})\cos\left(\frac{\omega_{\text{eff}}\Delta_\alpha}{2}\right) - (1+e^{i\alpha})\cos(\theta)\sin\left(\frac{\omega_{\text{eff}}}{2}\right)\right)}{2\sqrt{1-\left(\cos\left(\frac{\alpha}{2}\right)\cos\left(\frac{\omega_{\text{eff}}\Delta_\alpha}{2}\right) - \cos(\theta)\sin\left(\frac{\alpha}{2}\right)\sin\left(\frac{\omega_{\text{eff}}\Delta_\alpha}{2}\right)\right)^2}} \tag{B.8}$$

The components along x,y,z of $\mathbf{n}^{35}$ are:

$$n_x^{35} = -\frac{\sqrt{2}\cos\left(\frac{\alpha}{2}\right)\sin(\theta)\sin\left(\frac{\omega_{\text{eff}}\Delta_\alpha}{2}\right)}{\sqrt{2 - 2\cos\left(\frac{\alpha}{2}\right)^2\cos\left(\frac{\omega_{\text{eff}}\Delta_\alpha}{2}\right)^2 + (1-\cos(\alpha))\cos(\theta)^2\sin\left(\frac{\omega_{\text{eff}}}{2}\right)^2 - \cos(\theta)\sin(\alpha)\sin(\omega_{\text{eff}}\Delta_\alpha)}}$$

$$n_y^{35} = -\frac{\sqrt{2}\sin\left(\frac{\alpha}{2}\right)\sin(\theta)\sin\left(\frac{\omega_{\text{eff}}\Delta_\alpha}{2}\right)}{\sqrt{2 - 2\cos\left(\frac{\alpha}{2}\right)^2\cos\left(\frac{\omega_{\text{eff}}\Delta_\alpha}{2}\right)^2 + (-1+\cos(\alpha))\cos(\theta)^2\sin\left(\frac{\omega_{\text{eff}}}{2}\right)^2 - \cos(\theta)\sin(\alpha)\sin(\omega_{\text{eff}}\Delta_\alpha)}}$$

$$n_z^{35} = \frac{e^{\frac{-i\alpha}{2}}\left(i(-1+e^{i\alpha})\cos\left(\frac{\omega_{\text{eff}}\Delta_\alpha}{2}\right) + (1+e^{i\alpha})\cos(\theta)\sin\left(\frac{\omega_{\text{eff}}\Delta_\alpha}{2}\right)\right)}{\sqrt{2}\sqrt{2 - 2\cos\left(\frac{\alpha}{2}\right)^2\cos\left(\frac{\omega_{\text{eff}}\Delta_\alpha}{2}\right)^2 + (-1+\cos(\alpha))\cos(\theta)^2\sin\left(\frac{\omega_{\text{eff}}}{2}\right)^2 - \cos(\theta)\sin(\alpha)\sin(\omega_{\text{eff}}\Delta_\alpha)}} \tag{B.9}$$

B.5. Parameters determination

Eqs. (B.8) and (B.9) provide the general expression for the axes orientation in the subspaces 17 and 35. The experimentalist has the freedom to set up the value for the parameters Δ_α and α, whereas θ and ω_{eff} depend on the J coupling network of the system under analysis. Different choices of the Δ_α and α parameters impact on the orientation of the rotation axes in each subspace producing different rotations of the initial vectors I_z^{17} and $-I_z^{35}$.

The proposed parameters optimization is a three-step process:

1. Choose the angle α
2. Determine the optimal Δ_α so to move the rotation axis $\mathbf{n}^{35}$ into the transverse plane of the 35 subspace:

$$n_{35}^z(\alpha, \Delta_\alpha, \theta, \omega_{\text{eff}}) = 0 \quad \text{for some} \quad \Delta_\alpha = \Delta_{\alpha_{\text{opt}}} \tag{B.10}$$

3. Adjust the number of loops m^{17} and m^{35} so to achieve the highest projection $|I_z^{17} + I_z^{35}|$:

$$m^{17} = \frac{2k\pi}{\delta^{17}} \quad \text{for some integer k}$$
$$m^{35} = \frac{\pi}{\delta^{35}} \tag{B.11}$$

depending on the ratio m^{35}/m^{17}:

$$m_{\text{opt}} = m^{35} \quad \text{if} \quad \text{Round}\left(\frac{m^{35}}{m^{17}}\right) > 1 \quad \text{near equivalence}$$
$$m_{\text{opt}} = \text{Round}\left(\frac{m^{17}+m^{35}}{2}\right) \quad \text{otherwise} \tag{B.12}$$

where the subscript opt refers to the optimized value of the corresponding parameter and the dependence of n_{35}^z on $\alpha, \Delta_\alpha, \theta, \omega_{\text{eff}}$ has been made explicit. The integer k in Eq. (B.11) is chosen to return a value of m^{17} as close to m^{35} as possible. The angle α can be modified and the whole procedure repeated if necessary. Essentially α and Δ_α are chosen to move the rotation axis $\mathbf{n}^{35}$ on the transverse xy plane in the 35 subspace. The consequent choice of m_{opt} produces a $\simeq 2k\pi$ (for some $k = 1,2,\ldots$) rotation of I_z^{17} about the axis $\mathbf{n}^{17}$, and a $\simeq \pi$ rotation of $-I_z^{35}$ about the axis $\mathbf{n}^{35}$.

In the limit of $\theta \ll 1$ (near magnetic equivalence regime) the expressions of α and Δ_α have also been reported in Table 1. If the system is strongly inequivalent and $\theta \to \pi/2$ then ADAPT$_\alpha$ is not an extremely efficient method of transferring polarization and the best choice of m may return less than 90% polarization transfer.

B.6. Polarization

The heteronuclear polarization as a function of the number of repetitions m_{opt} is:

$$P(m_{opt}) = \frac{1}{2}\left(I_z^{17} \cdot \widehat{R}_{\mathbf{n}}^{17}(m_{opt}\delta^{17}) \cdot I_z^{17} + I_z^{35} \cdot \widehat{R}_{\mathbf{n}}^{35}(m_{opt}\delta^{35}) \cdot -I_z^{35}\right) \tag{B.13}$$

Intuitively in the near equivalence regime when $\theta \ll 1, n_z^{17}$ is only slightly tilted from the vertical axis of the subspace 17, and as a result the rotation about this axis gives a high z-projection almost irrespective on the number m of loops performed by ADAPT$_\alpha$ (see Fig. B.9c).

However in the far from equivalence regime, the angle formed by the axis $\mathbf{n}^{17}$ with the vertical axis can be very large, meaning that the vector I_z^{17} can be significantly tilted away from the vertical axis (see Fig. B.9a). Typically under this regime is worth considering small flip angle pulses and a higher number of repetition loops to be calculated as m_{opt}.

B.7. Duration

The duration of the pulse sequence, neglecting the short pulse duration (in the μs range), is simply the duration of the interval Δ_α multiplied for the number of repetitions m. Therefore, once the optimization process has been completed, the duration is calculated as:

$$\text{duration} = \Delta_{\alpha_{opt}} \times m_{opt} \tag{B.14}$$

B.8. Example

As an example let us consider TMVS (trimethylvinylsilane). We use the J coupling network in Hz units reported in Ref. [34]: $J_{12} = 14.6, J_{13} = 15.3, J_{23} = 6.5$. The system, according to Eq. (A.8), is described by the following parameters: $\theta = 0.2927$ and $\omega_{eff} = 95.8098$ rad s^{-1}. The steps to follow are:

1. set the angle. For example $\alpha = \frac{\pi}{2}$
2. the parameter Δ_{90} can be numerically determined solving the equation $n_{35}^z = 0$. The solution is $\Delta_{90} = 16.84$ ms.
3. the effective angles can be obtained resolving Eqs. (B.6) and (B.7): $\delta^{35} = 0.4199$ and $\delta^{17} \simeq \pi$. This leads to $m^{17} = 8.0024$ and $m^{35} = 7.48176$ for $k = 4$. We have chosen $m_{opt} = 8$
4. The theoretical polarization is 98.8% calculated by Eqs. (B.6) and (B.7)
5. The total duration is ∼134 ms

B.9. $\alpha = \pi$

As a special case, let us consider $\alpha = \pi$: ADAPT$_{180}$ becomes a train of π pulses. It can be verified that the rotation axes are:

$$\begin{aligned}\mathbf{n}^{17} &= \mathbf{n}^{35} \\ &= \left\{0, -\frac{\sin(\theta)\sin(\omega_{eff}\Delta_\alpha/2)}{\sqrt{1-\cos^2(\theta)\sin^2(\omega_{eff}\Delta_\alpha/2)}}, \right. \\ &\quad \left. -\frac{\cos(\omega_{eff}\Delta_\alpha/2)}{\sqrt{1-\cos^2(\theta)\sin^2(\omega_{eff}\Delta_\alpha/2)}}\right\}\end{aligned} \tag{B.15}$$

As a result I_z^{17} and $-I_z^{35}$ are rotated so to remain always the mirror image of one another, and no heteronuclear conversion is to be expected for an ADAPT$_{180}$ independently on Δ_α and the number of cycles used. Eq. (B.15) assumes a perfectly homogeneous B_1 field. If that is not the case, some significant conversion can still be attained for some values of Δ_α and m.

B.10. Geometrical evolution

The effective rotation of $m\delta_{eff}^{17}$ and $m\delta_{eff}^{35}$ about the axes $\mathbf{n}^{17} = \{n_x^{17}, n_y^{17}, n_z^{17}\}$ and $\mathbf{n}^{35} = \{n_x^{35}, n_y^{35}, n_z^{35}\}$ produced by an optimized m-cycle ADAPT$_\alpha$ sequence, results in a selective inversion in the 35 subspace.

The number of loops to achieve the close to 100% polarization transfer has to simultaneously rotate the vector $-I_z^{35}$ by $\sim \pi$ angle in the 35 subspace and also to determine a $\sim 2k\pi$ rotation in the 17 subspace, for some integer k, in order to achieve the highest value of the projection $|I_z^{17} + I_z^{35}| \propto I_{3x}$ (see also panels (a)–(d) in Fig. B.9).

Depending on the θ angle and on the effective frequency ω_{eff}, large or small flip angle pulses serve the purpose. As an approximate rule, 90° (or larger) pulses can be used in the near equivalence regime, like in Fig. B.9c and d, whereas small flip angles are indicated in general and when it is a poor approximation to consider $\theta \ll 1$, like in Fig. B.9a and b. When the flip angle α is sufficiently small ADAPT$_\alpha$ becomes a DANTE pulse sequence [37,40] capable to promote heteronuclear polarization transfer.

B.11. Off-resonance conversion bands

The underlying assumption of the theoretical analysis is that the ^{13}C pulses are applied on resonance. However, this might not always be the case, and in some low magnetic field parahydrogen experiments the exact control of the heteronuclear offset might not be trivial.

In presence of an off-resonance irradiation on the ^{13}C spin in addition to $\mathcal{H}_J$ the following term should be considered:

$$\begin{aligned}\mathcal{H}_{RF,off} &= \omega_{RF} I_{3x} + \omega_{off} I_{3z} \\ &= \omega_\phi \widehat{R}_y(\theta_{off}) I_{3z} \\ \theta_{off} &= \arctan\left(\frac{\omega_{RF}}{\omega_{off}}\right) \\ \omega_\phi &= \sqrt{\omega_{off}^2 + \omega_{RF}^2}\end{aligned} \tag{B.16}$$

The formal analysis that has been performed above considering $\omega_{off} = 0$ and representing the coherent Hamiltonian in a double-rotating frame, could be reproduced for $\mathcal{H}_{RF,off}$ by choosing a frame tilted from the vertical direction by an angle θ_{off}. We will not attempt such an analysis here but rather qualitatively justify the presence of conversion bands detected in experiments of Fig. 4 and simulations in Fig. 6 providing a practical recipe to predict their position.

Let us consider for simplicity a single-cycle ADAPT$_\alpha$ formed by a RF pulse and a delay. If the initial operator upon parahydrogenation is the proton scalar order, it will not be affected by the ^{13}C pulse. Subsequently during the free evolution delay, no RF irradiation is present and only the z component of $\mathcal{H}_{RF,off}$ in Eq. (B.16) can be considered.

Although in general $\mathcal{H}_{RF,off}$ in Eq. (B.16) does not commute with $\mathcal{H}_J$ for the presence of transverse RF components, in absence of RF pulses the evolution under J-coupling and under the offset Hamiltonian $\omega_{off} I_{3z}$ can be considered in any order as $[\omega_{off} I_{3z}, \mathcal{H}_J] = 0$. We can obtain the state of the system, after one cycle, by propagating the on-resonance state upon the action of the evolution operator:

$$\exp(-i\omega_{off}\Delta_\alpha I_{3z}) = \widehat{R}_{3z}(\omega_{off}\Delta_\alpha) \tag{B.17}$$

As a result the vectors I_z^{17} and I_z^{35} will then be transformed after one cycle into:

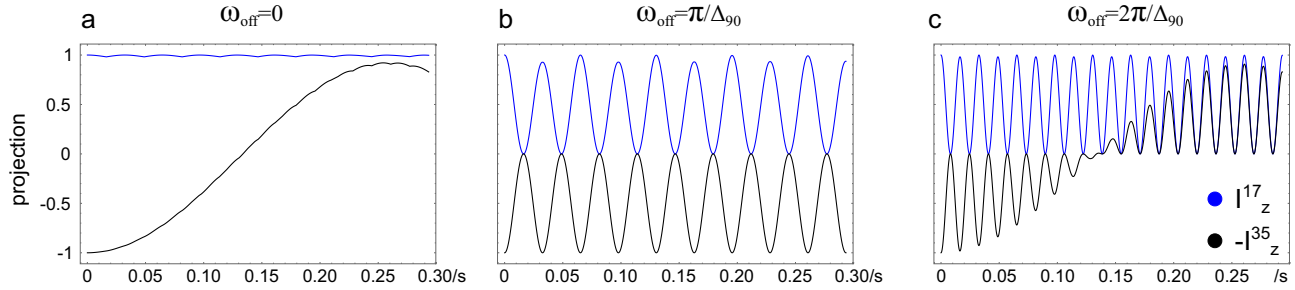

Fig. B.10. Fumaric acid trajectories of the vectors I_z^{17} in blue and $-I_z^{35}$ in black under ADAPT$_{90}$ for: (a) on resonance ^{13}C irradiation, (b) off-resonance ^{13}C irradiation $1/\Delta_{90} = 30.6$ Hz between the on resonance and the first conversion band and in (c) at $1/(2\Delta_{90}) = 61.3$ Hz away from resonance at the centre of the first conversion band. The ADAPT parameters are the same used in the experiments in Fig. 4: $\Delta_{90} = 16.3$ ms and $m = 18$.

$$\begin{aligned}\widehat{R}_{3z}(\omega_{off}\Delta_\alpha)\cdot I_z^{17}\cdot\widehat{R}_{3z}(-\omega_{off}\Delta_\alpha) &= I_z^{17} \quad \text{if} \quad \omega_{off}\Delta_\alpha = 2k\pi \\ &= -I_z^{35} \quad \text{if} \quad \omega_{off}\Delta_\alpha = \pi + 2k\pi \\ \widehat{R}_{3z}(\omega_{off}\Delta_\alpha)\cdot -I_z^{35}\cdot\widehat{R}_{3z}(-\omega_{off}\Delta_\alpha) &= -I_z^{35} \quad \text{if} \quad \omega_{off}\Delta_\alpha = 2k\pi \\ &= I_z^{17} \quad \text{if} \quad \omega_{off}\Delta_\alpha = \pi + 2k\pi\end{aligned} \tag{B.18}$$

Whenever $\omega_{off}\Delta_\alpha = 2k\pi$ for some integer k, the off-resonance evolution under scalar couplings would lead to the same on-resonance results already presented (see also Fig. B.10a and c).

When $\omega_{off}\Delta_\alpha = \pi + 2k\pi$ for any integer k the vectors I_z^{17} and $-I_z^{35}$ are transformed onto subspaces 35 and 17 respectively. Therefore the projection of the transformed vectors into their original subspace is zero. In practice, no conversion is expected for an off-resonance irradiation such that $\omega_{off}\Delta_\alpha = \pi + 2k\pi$ for any integer k (see Fig. B.10b). In the intermediate case, the vectors I_z^{17} and $-I_z^{35}$ will evolve under J-coupling in a way that depends on the resonance offset, the evolution delay and also the angle α.

The important experimental parameter is represented by the distance between consecutive conversion bands: $\omega_{off}\Delta_\alpha = 2\pi$. For near-equivalent systems one can choose an angle α as large as possible. In this way the conversion bands are closer to one another and possible off-resonance problems are mitigated, but never eliminated with the current strategy. This is experimentally confirmed in Fig. 4 for fumaric acid and in simulations in Fig. 6 for dimethyl maleate-d_6.

References

[1] C.R. Bowers, D.P. Weitekamp, Transformation of symmetrization order to nuclear-spin magnetization by chemical reaction and nuclear magnetic resonance, Phys. Rev. Lett. 57 (21) (1986) 2645–2648, http://dx.doi.org/10.1103/PhysRevLett.57.2645.

[2] T.G. Walker, W. Happer, Spin-Exchange Optical Pumping of Noble-Gas Nuclei (1997), http://dx.doi.org/10.1103/RevModPhys.69.629.

[3] J. Bargon, The Discovery of Chemically Induced Dynamic Polarization (CIDNP), Helv. Chim. Acta 89 (10) (2006) 2082–2102, http://dx.doi.org/10.1002/hlca.200690199. <http://www.pnas.org/cgi/content/long/100/18/10158>.

[4] S.B. Duckett, R.E. Mewis, Application of parahydrogen induced polarization techniques in NMR spectroscopy and imaging, Acc. Chem. Res. 45 (8) (2012) 1247–1257, http://dx.doi.org/10.1021/ar2003094. <http://www.ncbi.nlm.nih.gov/pubmed/22452702>.

[5] J.H. Lee, Y. Okuno, S. Cavagnero, Sensitivity enhancement in solution NMR: emerging ideas and new frontiers, J. Magn. Reson. 241 (2014) 18–31, http://dx.doi.org/10.1016/j.jmr.2014.01.005. <http://www.ncbi.nlm.nih.gov/pubmed/24656077>.

[6] K.L. Ivanov, A.N. Pravdivtsev, A.V. Yurkovskaya, H.-M. Vieth, R. Kaptein, The role of level anti-crossings in nuclear spin hyperpolarization, Prog. Nucl. Magn. Reson. Spectrosc. 81 (2014) 1–36, http://dx.doi.org/10.1016/j.pnmrs.2014.06.001. <http://linkinghub.elsevier.com/retrieve/pii/S0079656514000454>.

[7] J. Kurhanewicz, D.B. Vigneron, K. Brindle, E.Y. Chekmenev, A. Comment, C.H. Cunningham, R.J. Deberardinis, G.G. Green, M.O. Leach, S.S. Rajan, R.R. Rizi, B.D. Ross, W.S. Warren, C.R. Malloy, Analysis of cancer metabolism by imaging hyperpolarized nuclei: prospects for translation to clinical research, Neoplasia 13 (2) (2011) 81–97, http://dx.doi.org/10.1593/neo.101102. <http://www.pubmedcentral.nih.gov/articlerender.fcgi?artid=3033588&tool=pmcentrez&rendertype=abstract>.

[8] M. Karlsson, A. Gisselsson, S.K. Nelson, T.H. Witney, S.E. Bohndiek, G. Hansson, T. Peitersen, M.H. Lerche, K.M. Brindle, Production of hyperpolarized [1,4-13C2]malate from [1,4-13C2] fumarate is a marker of cell necrosis and treatment response in tumors, Proc. Natl. Acad. Sci. U.S.A. 106 (47) (2009) 19801–19806.

[9] K.M. Brindle, S.E. Bohndiek, F.a. Gallagher, M.I. Kettunen, Tumor imaging using hyperpolarized ^{13}C magnetic resonance spectroscopy, Magn. Reson. Med. 66 (2) (2011) 505–519, http://dx.doi.org/10.1002/mrm.22999. <http://www.ncbi.nlm.nih.gov/pubmed/21661043>.

[10] a. Lesage, M. Lelli, D. Gajan, M.a. Caporini, V. Vitzthum, P. Mieville, J. Alauzun, a. Roussey, C. Thieuleux, a. Mehdi, G. Bodenhausen, C. Coperet, L. Emsley, Surface enhanced NMR spectroscopy by dynamic nuclear polarization, J. Am. Chem. Soc. 132 (2010) 15459–15461, http://dx.doi.org/10.1021/ja104771z. <http://www.ncbi.nlm.nih.gov/pubmed/20831165>.

[11] A.J. Rossini, A. Zagdoun, M. Lelli, A. Lesage, C. Copéret, L. Emsley, Dynamic nuclear polarization surface enhanced NMR spectroscopy, Acc. Chem. Res. 46 (9) (2013) 1942–1951, http://dx.doi.org/10.1021/ar300322x.

[12] J. Natterer, J. Bargon, Parahydrogen induced polarization, Prog. Nucl. Magn. Reson. Spectrosc. 6565 (31) (1997) 293–315.

[13] R.a. Green, R.W. Adams, S.B. Duckett, R.E. Mewis, D.C. Williamson, G.G.R. Green, The theory and practice of hyperpolarization in magnetic resonance using parahydrogen, Prog. Nucl. Magn. Reson. Spectrosc. 67 (2012) 1–48, http://dx.doi.org/10.1016/j.pnmrs.2012.03.001. <http://www.ncbi.nlm.nih.gov/pubmed/23101588>.

[14] S. Glöggler, J. Colell, S. Appelt, Para-hydrogen perspectives in hyperpolarized NMR, J. Magn. Reson. 235 (2013) 130–142, http://dx.doi.org/10.1016/j.jmr.2013.07.010.

[15] J. Barkemeyer, J. Bargon, H. Sengstschmid, R. Freeman, Heteronuclear polarization transfer using selective pulses during hydrogenation with parahydrogen, J. Magn. Reson. Ser. A 120 (1) (1996) 129–132, http://dx.doi.org/10.1006/jmra.1996.0109. <http://linkinghub.elsevier.com/retrieve/pii/S1064185896901096>.

[16] M. Carravetta, O. Johannessen, M. Levitt, Beyond the T1 limit: singlet nuclear spin states in low magnetic fields, Phys. Rev. Lett. 92 (15) (2004) 153003, http://dx.doi.org/10.1103/PhysRevLett.92.153003.

[17] G. Pileio, M. Carravetta, E. Hughes, M.H. Levitt, The long-lived nuclear singlet state of 15N-nitrous oxide in solution, J. Am. Chem. Soc. 130 (38) (2008) 12582–12583, http://dx.doi.org/10.1021/ja803601d. <http://www.ncbi.nlm.nih.gov/pubmed/18729363>.

[18] M.H. Levitt, Singlet nuclear magnetic resonance, Annu. Rev. Phys. Chem. 63 (2012) 89–105, http://dx.doi.org/10.1146/annurev-physchem-032511-143724. <http://www.ncbi.nlm.nih.gov/pubmed/22224703>.

[19] B. Meier, J.-N. Dumez, G. Stevanato, J.T. Hill-Cousins, S.S. Roy, P. Håkansson, S. Mamone, R.C.D. Brown, G. Pileio, M.H. Levitt, Long-lived nuclear spin states in methyl groups and quantum-rotor-induced polarization, J. Am. Chem. Soc. 135 (50) (2013) 18746–18749, http://dx.doi.org/10.1021/ja410432f. <http://www.ncbi.nlm.nih.gov/pubmed/24252212>.

[20] S.S. Roy, J.-N. Dumez, G. Stevanato, B. Meier, J.T. Hill-Cousins, R.C.D. Brown, G. Pileio, M.H. Levitt, Enhancement of quantum rotor NMR signals by frequency-selective pulses, J. Magn. Reson. 250C (2014) 25–28, http://dx.doi.org/10.1016/j.jmr.2014.11.004. <http://www.sciencedirect.com/science/article/pii/S1090780714003024>.

[21] G. Stevanato, S. Singha Roy, J. Hill-Cousins, I. Kuprov, L.J. Brown, R.C.D. Brown, G. Pileio, M.H. Levitt, Long-lived nuclear spin states far from magnetic equivalence, Phys. Chem. Chem. Phys. 17 (8) (2015) 5913–5922, http://dx.doi.org/10.1039/C4CP05704J. <http://xlink.rsc.org/?DOI=C4CP05704J>.

[22] G. Stevanato, J.T. Hill-Cousins, S.S. Roy, L.J. Brown, R.C.D. Brown, G. Pileio, M.H. Levitt, A nuclear singlet lifetime of more than one hour in room-temperature solution, Angew. Chemie – Int. Ed. 54 (12) (2015) 3740–3743, http://dx.doi.org/10.1002/anie.201411978.

[23] S.J. Elliott, L.J. Brown, J.-N. Dumez, M.H. Levitt, Long-lived nuclear spin states in monodeuterated methyl groups, Phys. Chem. Chem. Phys. 18 (27) (2016) 17965–17972, http://dx.doi.org/10.1039/C6CP03619H.

[24] R. Sarkar, P.R. Vasos, G. Bodenhausen, Singlet-state exchange NMR spectroscopy for the study of very slow dynamic processes, J. Am. Chem. Soc. 129 (2) (2007) 328–334, http://dx.doi.org/10.1021/ja0647396. <http://www.ncbi.nlm.nih.gov/pubmed/17212412>.

[25] A. Bornet, X. Ji, D. Mammoli, B. Vuichoud, J. Milani, G. Bodenhausen, S. Jannin, Long-Lived States of Magnetically Equivalent Spins Populated by Dissolution-DNP and Revealed by Enzymatic Reactions, Chemistry http://dx.doi.org/10.1002/chem.201404967, <http://www.ncbi.nlm.nih.gov/pubmed/25346515>.

[26] W.S. Warren, E. Jenista, R.T. Branca, X. Chen, Increasing hyperpolarized spin lifetimes through true singlet eigenstates, Science 323 (5922) (2009) 1711–1714, http://dx.doi.org/10.1126/science.1167693. <http://www.pubmedcentral.nih.gov/articlerender.fcgi?artid=3080756&tool=pmcentrez&rendertype=abstract>.

[27] Y. Feng, R.M. Davis, W.S. Warren, Accessing long-lived nuclear singlet states between chemically equivalent spins without breaking symmetry, Nat. Phys. 8 (11) (2012) 831–837, http://dx.doi.org/10.1038/nphys2425. <http://www.pubmedcentral.nih.gov/articlerender.fcgi?artid=3596050&tool=pmcentrez&rendertype=abstract>.

[28] F. Reineri, T. Boi, S. Aime, ParaHydrogen Induced Polarization of ^{13}C carboxylate resonance in acetate and pyruvate, Nat. Commun. http://dx.doi.org/10.1038/ncomms6858.

[29] M. Goldman, H. Johannesson, Conversion of a proton pair para order into C-13 polarization by rf irradiation, for use in MRI, Comptes Rendus Phys. 6 (4-5) (2005) 575–581, http://dx.doi.org/10.1016/j.crhy.2005.03.002, <http://www.sciencedirect.com/science/article/pii/S1631070505000514\npapers2://publication/doi/10.1016/j.crhy.2005.03.002>.

[30] M. Goldman, H. Jóhannesson, O. Axelsson, M. Karlsson, Design and implementation of ^{13}C hyper polarization from para-hydrogen, for new MRI contrast agents, Comptes Rendus Chim. 9 (3–4) (2006) 357–363, http://dx.doi.org/10.1016/j.crci.2005.05.010. <http://linkinghub.elsevier.com/retrieve/pii/S1631074805002183>.

[31] L.T. Kuhn, J. Bargon, Transfer of Parahydrogen-Induced Hyperpolarization to Heteronuclei, in: In situ NMR Methods Catal., Springer Berlin Heidelberg, Berlin, Heidelberg, pp. 25–68. http://dx.doi.org/10.1007/128_064, <http://link.springer.com/10.1007/128_064>.

[32] G.A. Morris, R. Freeman, Enhancement of nuclear magnetic resonance signals by polarization transfer, J. Am. Chem. Soc. 101 (3) (1979) 760–762, http://dx.doi.org/10.1021/ja00497a058.

[33] M. Haake, J. Natterer, J. Bargon, Efficient NMR pulse sequences to transfer the parahydrogen-induced polarization to hetero nuclei, J. Am. Chem. Soc. 118 (36) (1996) 8688–8691, http://dx.doi.org/10.1021/ja960067f.

[34] S. Bär, T. Lange, D. Leibfritz, J. Hennig, D. von Elverfeldt, J.-B. Hövener, On the spin order transfer from parahydrogen to another nucleus, J. Magn. Reson. 225 (2012) 25–35, http://dx.doi.org/10.1016/j.jmr.2012.08.016. <http://linkinghub.elsevier.com/retrieve/pii/S1090780712002911>.

[35] S. Kadlecek, K. Emami, M. Ishii, R. Rizi, Optimal transfer of spin-order between a singlet nuclear pair and a heteronucleus, J. Magn. Reson. 205 (1) (2010) 9–13, http://dx.doi.org/10.1016/j.jmr.2010.03.004.

[36] S.J. DeVience, R.L. Walsworth, M.S. Rosen, Preparation of nuclear spin singlet states using spin-lock induced crossing, Phys. Rev. Lett. 111 (17) (2013) 173002, http://dx.doi.org/10.1103/PhysRevLett.111.173002, arXiv:1307.0832v1.

[37] G. Morris, R. Freeman, Selective excitation in Fourier transform nuclear magnetic resonance, J. Magn. Reson. 29 (3) (1978) 433–462, http://dx.doi.org/10.1016/0022-2364(78)90003-3.

[38] R. Freeman, G.A. Morris, The 'DANTE' experiment, J. Magn. Reson. 213 (2) (2011) 244–246, http://dx.doi.org/10.1016/j.jmr.2011.08.020.

[39] M.C.D. Tayler, M.H. Levitt, Accessing long-lived nuclear spin order by isotope-induced symmetry breaking, J. Am. Chem. Soc. 135 (6) (2013) 2120–2123, http://dx.doi.org/10.1021/ja312227h. <http://www.ncbi.nlm.nih.gov/pubmed/23360439>.

[40] D. Canet, J. Brondeau, C. Roumestand, Analytical expressions for the DANTE pulse sequence, J. Magn. Reson. Ser. A 117 (1) (1995) 103–108, http://dx.doi.org/10.1006/jmra.1995.9963. <http://linkinghub.elsevier.com/retrieve/pii/S1064185885799639>.

[41] M.C.D. Tayler, M.H. Levitt, Singlet nuclear magnetic resonance of nearly-equivalent spins, Phys. Chem. Chem. Phys. 13 (13) (2011) 5556–5560, http://dx.doi.org/10.1039/c0cp02293d. <http://www.ncbi.nlm.nih.gov/pubmed/21318206>.